Inorg. Chem. **2009**, *48*, 432−445

Synthesis and Characterization of Transition Metal Complexes of Dimeric N-Confused Porphyrin Linked by an *o*-Xylene Fragment

Piotr J. Chmielewski*

Department of Chemistry, University of Wrocław, 14 F. Joliot-Curie Street, 50-383 Wrocław, Poland

Received April 2, 2008

Insertion of nickel(II), zinc, cadmium, or silver(III) into both macrocyclic crevices of 2,2′-*o*-xylene-bis(5,10,15,20-tetrakis(*p*-tolyl)-2-aza-21-carbaporphyrin) results in homometallic dimeric complexes which were isolated and characterized by NMR, UV−vis, mass spectrometry, and cyclic voltammetry. The ^{1}H NMR study of these systems at low temperatures (203−233 K) allowed determination of most stable conformers with respect to a rotational freedom around the xylene bridge. An unfolded conformation for the dicationic bis(silver(III)) complex was determined on the basis of 2D nuclear Overhauser effect spectrometry experimentation. A mixture of nonequally populated diastereomers is observed for bis(zinc) and bis(cadmium) complexes due to a possibility of two different orientations of the apical anionic ligands with respect to the bridge. In a reaction of 5,10,15,20-tetrakis(*p*-tolyl)-2-aza-21-carbaporphyrinato nickel(II) with 2-(*o*-bromoxylene)-5,10,15,20-tetrakis(*p*-tolyl)-2-aza-21-carbaporphyrin in the presence of a proton scavenger, two isomeric bis(N-confused porphyrin) complexes with one subunit "empty" and the other metalated by nickel(II) were obtained. In the product **10**, the *o*-xylene links external nitrogens of the subunits while product **11** consists of the xylene bridge between external nitrogen of the nonmetalated subunit and internal carbon of the fragment containing a nickel(II) ion. The products were characterized by mass spectrometry, UV−vis, NMR, and, in the case of complex **11**, also by X-ray crystallographic analysis (space group $P\bar{1}$, a =17.007(3), b = 18.130(3), c = 18.797(2) Å, α = 105.856(13)°, β = 107.447(13)°, γ = 98.818(15)°, V = 5141.1(15) Å^3, Z = 2). Insertion of zinc or silver(III) into an empty crevice of **10** resulted in heterometallic zinc−nickel(II) or silver(III)−nickel(II) complexes **12** or **13**, respectively, which were characterized by NMR, UV−vis, and cyclic voltammetry. The subunits in the bis(porphyrin) systems retain spectroscopic and redox properties typical for monomeric complexes.

Introduction

N-confused (inverted) porphyrin (NCP) **1**[1–3] forms variety of stable organometallic compounds[4–12] displaying multimodal coordination properties (see Chart 1).[11–24] A peculiar reactivity of metal complexes[25] of NCP allows further modification of the system which involves the *confused* pyrrole[26–36] due to its susceptibility to various types of reaction. The free-base porphyrin also can be a subject of derivatization that leads to the formation of many species bearing substituents on the external nitrogen (N2),[37–41] external carbon (C3),[42–44] or internal carbon (C21).[45,46] The attractiveness of NCP and its complexes comes from its facile

* Author to whom correspondence should be addressed. E-mail: pjc@wchuwr.pl.

(1) Chmielewski, P. J.; Latos-Grażyński, L.; Rachlewicz, K.; Głowiak, T. *Angew. Chem., Int. Ed. Engl.* **1994**, *33*, 779–781.
(2) Furuta, H.; Asano, T.; Ogawa, T. *J. Am. Chem. Soc.* **1994**, *116*, 767.
(3) Geier, G. R., III; Haynes, D. M.; Lindsey, J. S. *Org. Lett.* **1999**, *1*, 1455.
(4) Furuta, H.; Ogawa, T.; Uwatoko, Y.; Araki, K. *Inorg. Chem.* **1999**, *38*, 2676.
(5) Ogawa, T.; Furuta, H.; Takahashi, M.; Morino, A.; Uno, H. *J. Organomet. Chem.* **2000**, *611*, 551.
(6) Maeda, H.; Ishikawa, Y.; Matsueda, H.; Osuka, A.; Furuta, H. *J. Am. Chem. Soc.* **2003**, *125*, 11822.
(7) Maeda, H.; Osuka, A.; Ishikawa, Y.; Aritome, I.; Hisaeda, Y.; Furuta, H. *Org. Lett.* **2003**, *5*, 1293.
(8) Liu, J.-C.; Ishizuka, T.; Osuka, A.; Furuta, H. *Chem. Commun.* **2004**, 1908.
(9) Chmielewski, P. J.; Latos-Grażyński, L. *Inorg. Chem.* **1997**, *36*, 840.
(10) Chmielewski, P. J.; Latos-Grażyński, L.; Schmidt, I. *Inorg. Chem.* **2000**, *39*, 5475.
(11) Harvey, J. D.; Ziegler, C. J. *Chem. Commun.* **2002**, 1942.
(12) Harvey, J. D.; Ziegler, C. J. *Chem. Commun.* **2004**, 1666.
(13) Harvey, J. D.; Ziegler, C. J. *Coord. Chem. Rev.* **2003**, *247*, 1.
(14) Chmielewski, P. J.; Latos-Grażyński, L. *Coord. Chem. Rev.* **2005**, *249*, 2510.
(15) Furuta, H.; Kubo, N.; Maeda, H.; Ishizuka, T.; Osuka, A.; Nanami, H.; Ogawa, T. *Inorg. Chem.* **2000**, *39*, 5424.
(16) Srinivasan, A.; Furuta, H.; Osuka, A. *Chem. Commun.* **2001**, 1666.
(17) Furuta, H.; Maeda, H.; Osuka, A. *Chem. Commun.* **2002**, 1795.

10.1021/ic800591n CCC: $40.75
Published on Web 06/21/2008

Chart 1

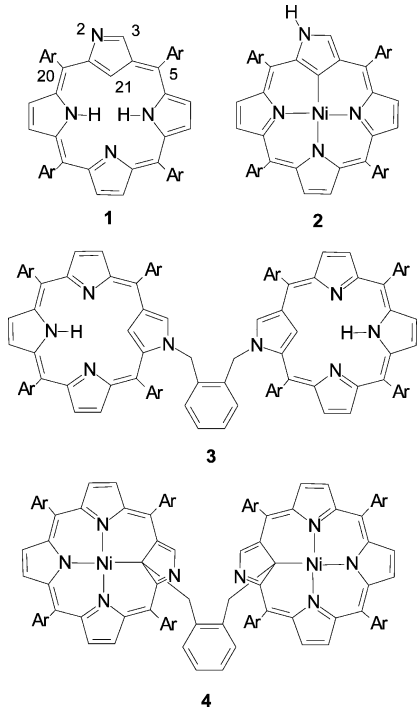

modification leading to the alteration of its coordination, redox, optical, and acid−base properties. Considering retention of the aromatic properties of the macrocyclic ring upon these modifications, NCP can be applied instead of the regular porphyrins in the potentially useful molecular[47,48] and supramolecular systems.[49–52] A built-in external coordinating site of **1** or some of its derivatives, that is, the exposed outer nitrogen of the *confused* pyrrole, has been shown to be involved in formation of the coordinately linked oligomers.[15,18–20,22,33,53–55] Also, a number of covalent dimers consisting of N-confused porphyrin subunits linked either directly[44,56] or by an alkanyl bridge[27,29,38] have been reported recently.

The present contribution is focused on the synthesis, characterization, and dynamics of the N-confused bisporphyrin complexes linked by an *o*-xylene fragment by using either nickel(II) complex **2**[1] as a substrate for dimerization reaction or by inserting metal ions into predefined dimeric ligand **3**, whose synthesis was described recently.[38] The resulting systems, covalently linked by such a semirigid bridge can adopt various orientations of the macrocyclic subunits and display interaction between these subunits depending on the way in which the fragments are connected and arranged. In the previous report, a face-to-face arrangement of the porphyrinoid subunits has been demonstrated both in the solid state and in solution for the system where *o*-xylene linked internal carbons of the *confused* pyrroles of bis(nickel(II)) complex **4**.[57] A relatively strong interaction between the subunits despite a lack of electronic delocalization suggested a mutual through-space influence of closely spaced porphyrinoid rings. The synthetic approaches applied in the present paper lead to the dimer consisting of the same, yet differently arranged, building blocks as those of **4** or allow the preparation of heterometallic systems.

Results and Discussion

Synthesis. The insertion of nickel(II) into dimeric ligand **3** (Scheme 1) yields symmetric diamagnetic neutral complex **5**, which is isomeric with **4**. Also, metalation of **3** by using silver(I) salt proceeds smoothly under mild conditions, leading to the formation of a first dicationic silver(III) complex **6** (Scheme 1). The dimeric character of this species is supported by the electrospray ionization mass spectrometry (ESI-MS) spectrum in which two peaks can be found: the one at $m/z = 827$ amu represents the dication, while the other at 1741 amu is attributable to the monocation that comprises

(18) Furuta, H.; Ishizuka, T.; Osuka, A. *J. Am. Chem. Soc.* **2002**, *124*, 5622.
(19) Furuta, H.; Youfu, K.; Maeda, H.; Osuka, A. *Angew. Chem., Int. Ed.* **2003**, *42*, 2186.
(20) Furuta, H.; Morimoto, T.; Osuka, A. *Inorg. Chem.* **2004**, *43*, 1618.
(21) Chen, W.-C.; Hung, C.-H. *Inorg. Chem.* **2001**, *40*, 5070.
(22) Hung, C.-H.; Chen, W.-C.; Lee, G.-H.; Peng, S.-M. *Chem. Commun.* **2002**, 1516.
(23) Rachlewicz, K.; Wang, S.-L.; Peng, C.-H.; Hung, C.-H.; Latos-Grażyński, L. *Inorg. Chem.* **2003**, *42*, 7348–7350.
(24) Toganoh, M.; Konagawa, J.; Furuta, H. *Inorg. Chem.* **2006**, *45*, 3852.
(25) Chmielewski, P. J.; Latos-Grażyński, L.; Głowiak, T. *J. Am. Chem. Soc.* **1996**, *118*, 5690.
(26) Chmielewski, P. J.; Latos-Grażyński, L. *Inorg. Chem.* **2000**, *39*, 5639.
(27) Schmidt, I.; Chmielewski, P. J.; Ciunik, Z. *J. Org. Chem.* **2002**, *67*, 8917.
(28) Schmidt, I.; Chmielewski, P. J. *Inorg. Chem.* **2003**, *42*, 5579.
(29) Schmidt, I.; Chmielewski, P. J. *Chem. Commun.* **2002**, 92.
(30) Xiao, Z.; Patrick, B. O.; Dolphin, D. *Chem. Commun.* **2002**, 1816.
(31) Xiao, Z.; Patrick, B. O.; Dolphin, D. *Chem. Commun.* **2003**, 1062.
(32) Xiao, Z.; Patrick, B. O.; Dolphin, D. *Inorg. Chem.* **2003**, *42*, 8125.
(33) Rachlewicz, K.; Wang, S.-L.; Ko, J.-L.; Hung, C.-H.; Latos-Grażyński, L. *J. Am. Chem. Soc.* **2004**, *126*, 4420–4431.
(34) Bohle, D. S.; Chen, W.-C.; Hung, C.-H. *Inorg. Chem.* **2002**, *41*, 3334.
(35) Hung, C.-H.; Wang, S.-L.; Ko, J.-L.; Peng, C.-H.; Hu, C.-H.; Lee, M.-T. *Org. Lett.* **2004**, *6*, 1393.
(36) Furuta, H.; Maeda, H.; Osuka, A. *Org. Lett.* **2002**, *4*, 181.
(37) Chmielewski, P. J.; Latos-Grażyński, L. *J. Chem. Soc., Perkin Trans. 2* **1995**, 503.
(38) Chmielewski, P. J. *Org. Lett.* **2005**, *7*, 1789.
(39) Qu, W.; Ding, T.; Cetin, A.; Harvey, J. D.; Taschner, M. J.; Ziegler, C. J. *J. Org. Chem.* **2006**, *71*, 811.
(40) Li, X.; Chmielewski, P. J.; Xiang, J.; Xu, J.; Li, Y.; Liu, H.; Zhu, D. *Org. Lett.* **2006**, *8*, 1137.
(41) Li, X.; Chmielewski, P. J.; Xiang, J.; Xu, J.; Jiang, L.; Li, Y.; Liu, H.; Zhu, D. *J. Org. Chem.* **2006**, *71*, 9739.
(42) Schmidt, I.; Chmielewski, P. J. *Tetrahedron Lett.* **2001**, *42*, 1151.
(43) Schmidt, I.; Chmielewski, P. J. *Tetrahedron Lett.* **2001**, *42*, 6389.
(44) Chmielewski, P. J. *Angew. Chem., Int. Ed.* **2004**, *43*, 5655.
(45) Ishikawa, Y.; Yoshida, I.; Akaiwa, K.; Koguchi, E.; Sasaki, T.; Furuta, H. *Chem. Lett.* **1997**, 453.
(46) Furuta, H.; Ishizuka, T.; Osuka, A.; Ogawa, T. *J. Am. Chem. Soc.* **1999**, *121*, 2945.
(47) Wojaczyński, J.; Latos-Grażyński, L. *Coord. Chem. Rev.* **2000**, *204*, 113.
(48) Burrell, A.; Officer, D. L.; Plieger, P. G.; Reid, D. C. W. *Chem. Rev.* **2001**, *101*, 2751.
(49) Atwood, J. L.; Davies, J. E.; MacNicol, D. D.; Vogtle, F. E. *Comprehensive Supramolecular Chemistry*; Pergamon: Oxford, U.K., 1996.
(50) Lehn, J.-M. *Supramolecular Chemistry: Concepts and Perspectives*; WCH: Wenheim, Germany, 1995.
(51) Wasielewski, M. R. *Chem. Rev.* **1992**, *92*, 435.
(52) D'Souza, F.; Smith, P. M.; Rogers, L.; Zandler, M. E.; Islam, D.-M. S.; Araki, Y.; Ito, O. *Inorg. Chem.* **2006**, *45*, 5057.
(53) Toganoh, M.; Harada, N.; Morimoto, T.; Furuta, H. *Chem.—Eur. J.* **2007**, *13*, 2257.
(54) Chmielewski, P. J.; Schmidt, I. *Inorg. Chem.* **2004**, *43*, 1885.
(55) Chmielewski, P. J. *Angew. Chem., Int. Ed.* **2005**, *44*, 6417.
(56) Ishizuka, T.; Osuka, A.; Furuta, H. *Angew. Chem., Int. Ed.* **2004**, *43*, 5077.
(57) Chmielewski, P. J. *Inorg. Chem.* **2007**, *46*, 1617.

Scheme 1

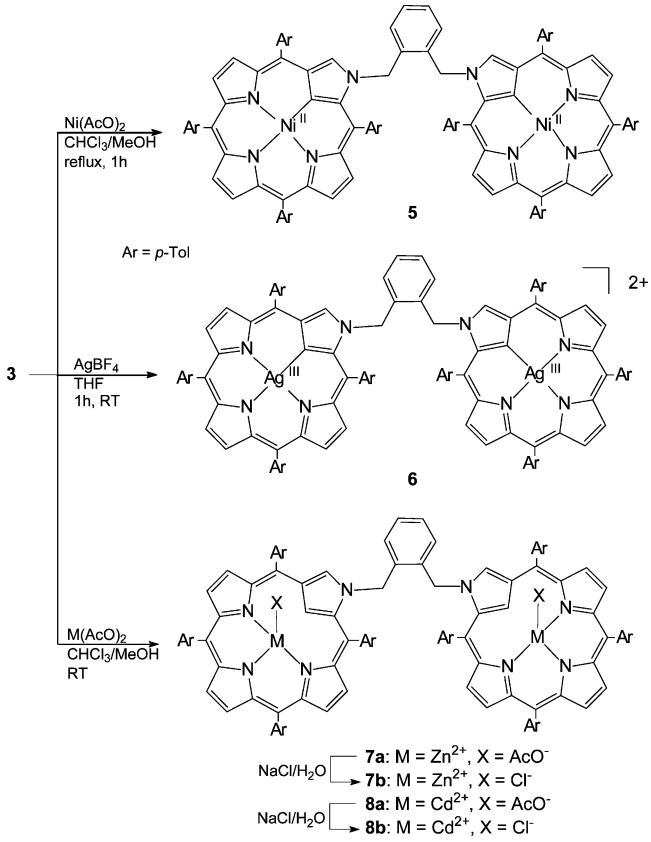

a tetrafluoroborate group associated with the dimer. It is noteworthy that **6** is stable despite only dianionic character of a coordination core in each of the linked subunits. With two exceptions,[38,58] in all known macrocyclic complexes of the trivalent silver the coordination core was trianionic, fully neutralizing the charge of the metal ion.[4,55,59–63]

The other homonuclear dimeric complexes, **7a** and **8a**, are immediately formed upon combining a chloroform solution of ligand **3** with an excess of zinc or cadmium acetate, respectively in methanol (Scheme 1). The labile apical acetate can be easily substituted by means of aqueous NaCl, which results in the formation of the chloride complexes **7b** and **8b**. The ESI-MS spectrum of **7b** consists of one peak at m/z = 1605.9 amu that is in line with the presence of a chloride ligand.

Two asymmetric isomeric bis(porphyrinic) systems are formed in a reaction of nickel(II) complex **2** with an equimolar amount of 2-bromoxylene-substituted NCP **9** (Scheme 2), whose synthesis has been reported recently.[38] Aapplication of a basic catalyst (K_2CO_3/[18]-crown-6 system) resulted in an approximately 70:30 mixture of **10** and **11** after about 3 h of refluxing the reaction mixture in THF. The ESI-MS spectra for both systems are identical, consisting of one peak at m/z = 1500 amu.

An insertion of zinc(II) or silver(III) into the "empty" macrocyclic subunit of **10** led to the formation of the heterometallic complexes **12** or **13**, respectively (Scheme 3). For both metals, the reaction takes place at room temperature. However, in the case of the silver complex, a paramagnetic species, likely containing a nickel(III) center, is formed initially. It is due to the oxidative properties of silver(I) salt with respect to the divalent nickel ion coordinated in the carbaporphyrinoid crevice.[9] The excess of $AgBF_4$ can be removed by washing the chloroform solution with a small amount of water, which allows the separation of **13**. The ESI-MS spectra for **12** (m/z = 1563 amu) and **13** (m/z = 1604 amu) confirm the heterometallic character of the complexes. The apical acetate in **12a** can be easily substituted with chloride by means of aqueous NaCl, which yields **12b**.

Spectroscopic Characterization. ^{1}H and ^{13}C NMR, including homo- and heteronuclear 2D techniques, were applied for characterization of the new compounds. The NMR of the NCP and its derivatives is particularly informative due to their low symmetry.[27,29,38,54] In the current systems, methylene protons of the xylene bridge constitute a diastereotopic probe providing additionally some information about the dynamics of the bis(porphyrin).

Spectral characteristics of **5** or **6** (Figure 1, traces A and B), due to their symmetric character, to some extent resemble those of monomeric nickel(II) or silver(III) complexes of NCP and its 2-substituted derivatives.[1,4,27,37,38] However, about a 0.5 ppm upfield shift of one of the tolyllic methyl signals in the ^{1}H NMR spectra of both complexes suggests a shielding influence of the aromatic ring current of the neighboring subunit on the resonance frequency. At room temperature, the methylene groups of the xylene bridge as well as protons within each of the CH_2 fragments are isochronous, although the signals at about 4.5 or 5.5 ppm in **5** or **6**, respectively, are significantly broadened. At temperatures below 233 K, the degeneracy of the methylene signals is removed by slowing down rotation around the C(Xyl)−N2 bond. It results in splitting of the methylene resonance into two broad signals in the spectrum of **5** (Figure 3A′) and into two doublets (^2J = 17.8 Hz) in that of **6** (Figure 3B′), indicating diastereotopic differentiation of the methylene protons. Significantly, no other signal splits that is in line with symmetric conformation of the dimers. It may be inferred from the comparison of ^{1}H NMR spectral data observed for **6** with those reported for the N-unsubstituted NCP complexes of trivalent silver that the electron density distributions among the pyrrole protons are similar despite the highly charged character of the bis(silver(III)) adduct.

Analysis of a nuclear Overhauser effect spectrometry (NOESY) spectrum of **6** recorded at 203 K for a carefully overcooled $CDCl_3$ solution reveals an unfolded conformation of the bis(porphyrinoid) system and allows a model to be built that takes into account observed interprotonic contacts between the subunits. The correlations that are most significant for the structure elucidation of **6** are marked in the NOESY map and on the chart presenting the model

(58) Pawlicki, M.; Latos-Grażyński, L. *Chem.—Eur. J.* **2003**, *9*, 4650.
(59) Furuta, H.; Maeda, H.; Osuka, A. *J. Am. Chem. Soc.* **2000**, *122*, 803.
(60) Muckey, M. A.; Szczepura, L. F.; Ferrence, G. M.; Lash, T. D. *Inorg. Chem.* **2002**, *41*, 4840.
(61) Lash, T. D.; Colby, D. A.; Szczepura, L. F. *Inorg. Chem.* **2004**, *43*, 5258.
(62) Lash, T. D.; Rasmussen, J. M.; Bergman, K. M.; Colby, D. A. *Org. Lett.* **2004**, *6*, 549.
(63) Bruckner, Ch.; Barta, Ch. A.; Brinas, R. P.; Krause-Bauer, J. A. *Inorg. Chem.* **2003**, *42*, 1673–1680.

Scheme 2

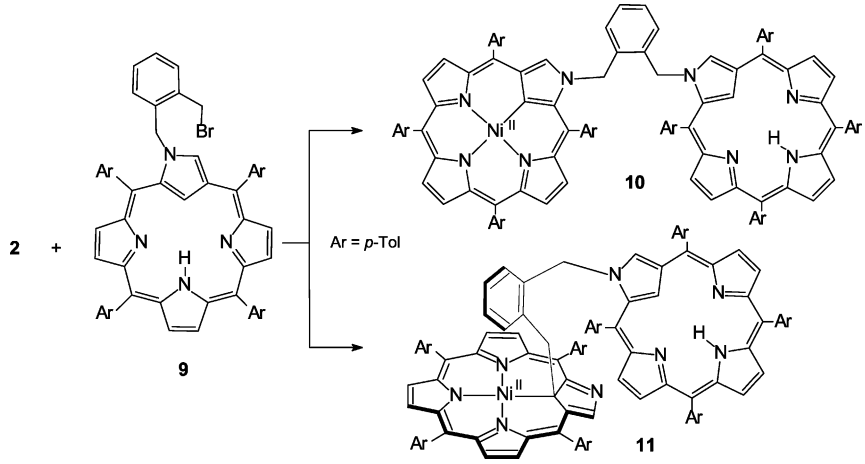

Scheme 3

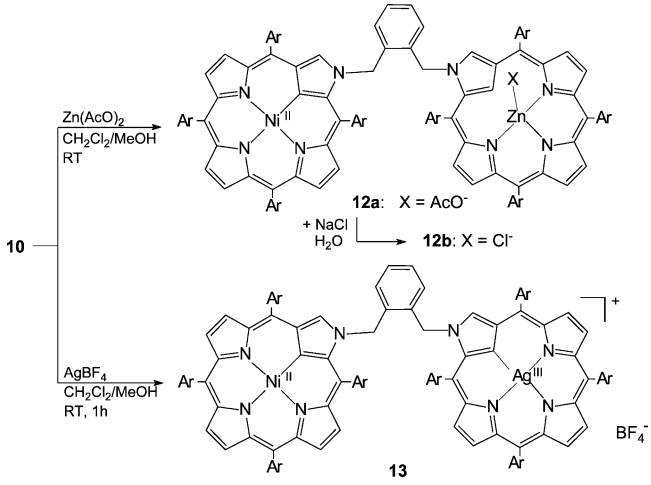

optimized by molecular mechanics in Figure 2. Among them are dipolar interactions of the methyl group of the tolyl substituent at position 20 with H3 (cross-peak A), with CH_2 protons of the xylene bridge (cross-peaks B), and with tolyllic CH_3 at the position 5 (cross-peak C), unequivocally indicating the way of mutual orientation of the subunits in solution.

In the case of heterometallic complex **13**, the asymmetric character of the compound is reflected by the appearance of two sets of β-pyrrole and *meso*-aryl resonances observed in the ^{1}H NMR spectrum ($CDCl_3$, 298 K, Figure 3C) as well as by a lack of degeneracy of the xylene bridge signals. The resonance positions of the respective protons in each of the

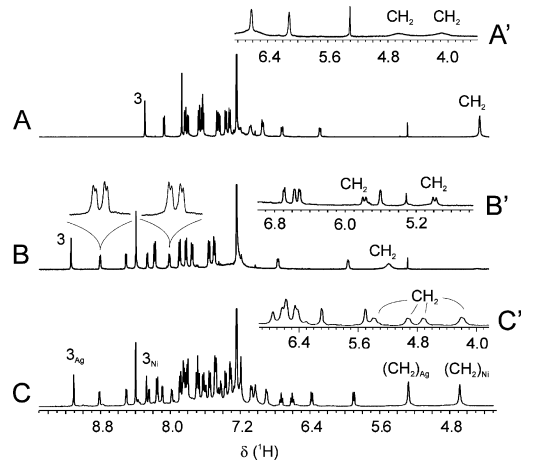

Figure 1. Low-field parts of the ^{1}H NMR spectra (500 MHz, $CDCl_3$) of **5** (A), **6** (B), and **13** (C) taken at 298 K. The expansions of two of the β-pyrrole resonances (components of an AB system) in trace B present signal splitting due to proton coupling with ^{107,109}Ag nuclei (^4J = 1.1 Hz). Insets A′, B′, and C′ show fragments of the ^{1}H NMR spectra of **5**, **6**, and **13**, respectively, recorded in overcooled $CDCl_3$ at 203 K.

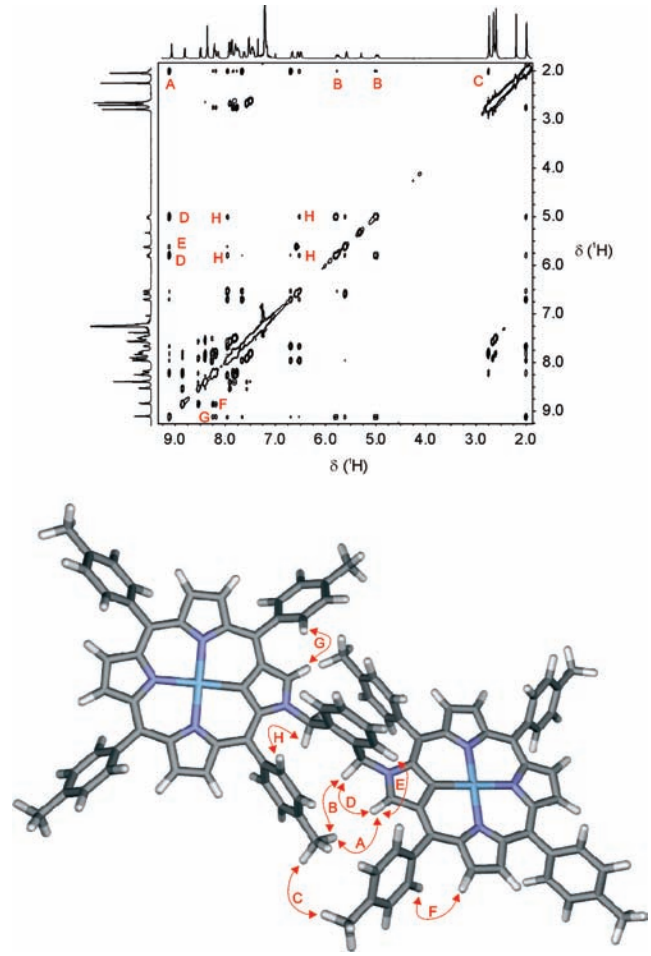

Figure 2. NOESY spectrum (top, 500 MHz, overcooled $CDCl_3$, 203 K) and an energy-minimized model of **6** (bottom). The cross-peak assignments in the map (A−H) indicate interprotonic interaction marked on the model by curved arrows.

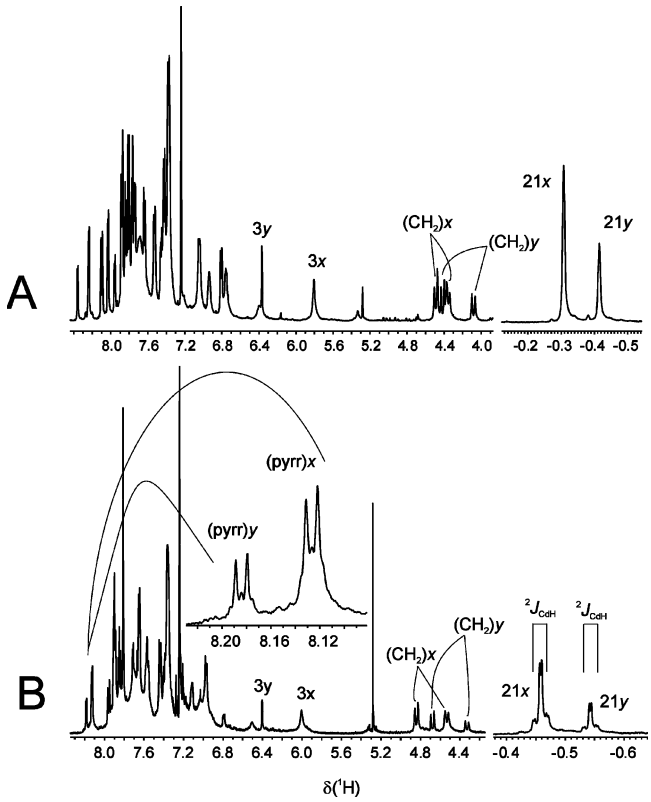

Figure 3. Fragments of ^{1}H NMR spectra ($CDCl_3$, 298 K) of **7b** (A) and **8a** (B). The indices *x* and *y* in the peak assignments are introduced to distinguish signals of diastereomers. The extension of two β-pyrrole signals in trace B and sticks in the high-field part of this spectrum present a fine structure of the peaks with satellites due to a coupling with ^{111,113}Cd nuclei.

subunits of **13** are similar to those observed in the symmetric dimers **5** and **6**, indicating a lack of the essential alteration in the electronic structure of the subunits. Also, in this case, at low temperatures, both methylene groups of the xylene bridge are diastereotopic (203 K, overcooled $CDCl_3$, Figure 1C′). The arrangement of the silver(III)- and nickel(II)-containing subunits seems to be analogous to that in **6**, which can be inferred from a room-temperature NOESY spectrum in which protons in the 3 positions (3_{Ag} and 3_{Ni} in Figure 1) correlate with most upfield-shifted CH_3 signals of tolyl substituents.

The ^{1}H NMR spectra of zinc and cadmium dimeric complexes **7** and **8** (Figure 3) indicate the presence of a proton bound to the internal carbon of the *confused* pyrrole and a side-on coordination of the trigonal-hybridized C21. A splitting of the 21-CH proton signals in the ^{1}H NMR spectra of **8** due to ^{1}H−^{111,113}Cd coupling is in line with a bonding interaction between internal carbon and the metal ion. Also, the position of the C21 signal found in the ^{1}H−^{13}C HMQC maps of **7** and **8** (∼76 ppm) is strongly shifted upfield with respect to that of the free ligand (109.1 ppm),[38] suggesting changes in electron density on this carbon atom due to the formation of a weak bond. These features are characteristic for Zn^{2+} or Cd^{2+} coordination to carbaporphyrinoids.[10,18,20,53,64–66] As a result of such a coordination mode, the subunits of the dimers are nonplanar, which leads to its chirality resulting in a diastereotopic differentiation of the methylene protons of the xylene bridge in the complexes of both metals. Unlike in the cases of **5** and **6**, where the macrocyclic subunits are planar, the differentiation in **7** and **8** cannot be dynamically averaged by rotation, and thus it is observed also at room temperature. Another consequence of local chirality of the subunits is the observation of two sets of signals in the ^{1}H NMR spectra of **7** and **8**, which is related to the presence of diastereomers. One set of signals can be assigned to a mixture of enantiomers which are not distinguishable by NMR, with the same *RR* or *SS* configurations of both subunits, while the other set represents the meso form consisting of heterochiral subunits. The diastereomers are not equally populated either for zinc or for cadmium complexes. The molar ratio of the isomers is about 1:2 for **7b** and **8a** and 1:4 for **8b**. Clearly, there is a steric preference for one of the stereoisomers. As expected, no equilibrium between the diastereomers occurs. Their molar ratios do not depend on temperature, and no chemical exchange correlation signals between the respective protons of the isomers are observed in the NOESY or rotating-frame Overhauser enhancement spectroscopy (ROESY) experiments. Unlike in the cases of **5**, **6**, and **13**, there is no correlation of any of the H3 with tolyllic CH_3 in the NOESY spectra of **7b** and **8b**. It may suggest different spatial arrangement of the subunits in the case of zinc or cadmium complexes than that proposed for the former systems.

The conformational space analyzed for **7b** and **8b** by means of molecular mechanics and the semiempirical PM3 method for these stereoisomers involves several energy minima consisting of rotamers which differ from each other by an orientation of the apical anion with respect to the vector defined by the phenylene part of the xylene bridge (Scheme 4). Thus, the chloride ligands can be situated both on the same side of the mean plane of the system as the phenylene fragment (R_uR_u, S_uS_u, S_uR_u) or both on the opposite side (R_dR_d, S_dS_d, S_dR_d) of the phenylene ring or can adopt alternating directions with respect to that of the bridge (R_dR_u, S_dS_u, S_dR_u, S_uR_d). The relative energy values for PM3 energy-optimized models of the conformers of each stereoisomer of **8b** are presented in Scheme 4. At room temperature, rotation around the bonds of the xylene bridge, which is fast on the NMR time scale, averages the magnetic environment of protons, and thus the effective symmetry of each diastereomer is 2-fold, resulting in a degeneracy of the signals of the subunits. At lower temperatures (233−203 K), the signals are broadened and eventually split, which reflects differentiation of the resonances due to slowing down the rotation at the bridge. In the case of bis(chlorocadmium) complex **8b**, the spectral lines of the more populated diastereomer are sufficiently sharp to allow an analysis of the spectrum at 213 K, while signals of the minor isomer are still broad (Figure 4A). The two sets of signals of equal intensity can be related either to the presence of two equally populated

(64) Siczek, M.; Chmielewski, P. J. *Angew. Chem., Int. Ed.* **2007**, *46*, 7432.
(65) Furuta, H.; Ishizuka, T.; Osuka, A. *Inorg. Chem. Commun.* **2003**, *6*, 398.
(66) Stępień, M.; Latos-Grażyński, L.; Szterenberg, L.; Panek, J.; Latajka, Z. *J. Am. Chem. Soc.* **2004**, *126*, 4566–4580.

Scheme 4

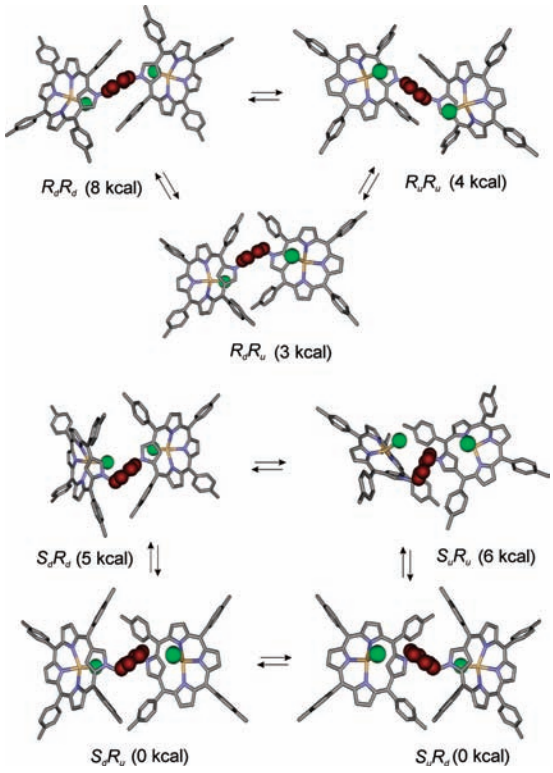

"symmetric" conformers which differ in orientation with respect to the bridge (R_uR_u/R_dR_d and enantiomeric S_uS_u/S_dS_d) or to a magnetic inequivalence of subunits in a system of asymmetric structure (S_uR_u, S_dR_d R_dR_u, S_dS_u, S_dR_u, S_uR_d). The NOESY and ROESY experiments can be operative in distinguishing between these two situations. Since the differentiation of signals at low temperatures is caused by the slowing down of the dynamic processes (rotation), by necessity all corresponding protons of different sets (e.g., H21, H3, bridging CH_2) correlate in the NOESY spectrum, giving strong chemical exchange signals (EXSs). In the case of two different rotamers, only this type of correlation should be observed for the respective protons of the isomers and no NOE (i.e., correlation effect due to a spatial proximity of protons) between them should take place, while in the asymmetric dimer, the particular protons of its different "halves" (e.g., protons of different methylene groups at the xylene bridge) are close enough to each other to give a NOE signal. The ROESY spectrum discriminates between EXS and ROE (i.e., rotating frame Overhauser effect) through a different phase of cross-peaks: these, due to chemical exchange and scalar interactions, have the same phase as a diagonal, while ROE signals have the opposite phase. All correlations observed in the NOESY map should appear in the ROESY experiment if interaction between protons has a unique character (i.e., exclusively scalar, ROE, or EXS), as is expected for the mixture of rotamers. If, however, protons interact simultaneously by a through-space coupling and by chemical exchange or scalar coupling, their correlation peak may be weakened or even absent in the ROESY map, being a result of superposition of the opposite phase effects. The latter situation takes place in the actual ROESY experiment performed for **8b** at 213 K (Figure 4B). There is no correlation among four signals of methylene protons of bridging xylene, although they correlate (ROE) with H3, bridging phenylene, or *meso*-aryl protons. Moreover, a scalar coupling pattern in a correlation spectroscopy (COSY) experiment at 213 K indicates the presence of a unique set of xylene protons expected for an asymmetric dimer. The magnetic nonequivalency of the subunits excludes symmetric conformers with homochiral subunits as a major component of the diastereomeric mixture of **8b**. Also, the lack of H3 interactions with the tolyllic methyl protons, which can be predicted on the basis of molecular models of the symmetric conformers R_uR_u, S_uS_u, R_dR_d, or S_dS_d, for which the mean values of the appropriate interprotonic distances are about 3 Å, is in line with the domination of one of the asymmetric rotamers. Similarly, an absence of the expected strong correlations between protons of the tolyl substituents in the 5 and 20 positions of different subunits excludes heterochiral diastereomer S_dR_u/R_dS_u, though its relative energy is the lowest according to the PM3 calculations. A pattern of the interprotonic interaction for H3 on both subunits as well as an about 0.6 ppm upfield shift of the methyl protons of the 20-tolyl substituents suggest the structure of asymmetric system R_uR_d/S_uS_d and, thus, domination of the diastereomer of homochiral subunits in the case of **8b**.

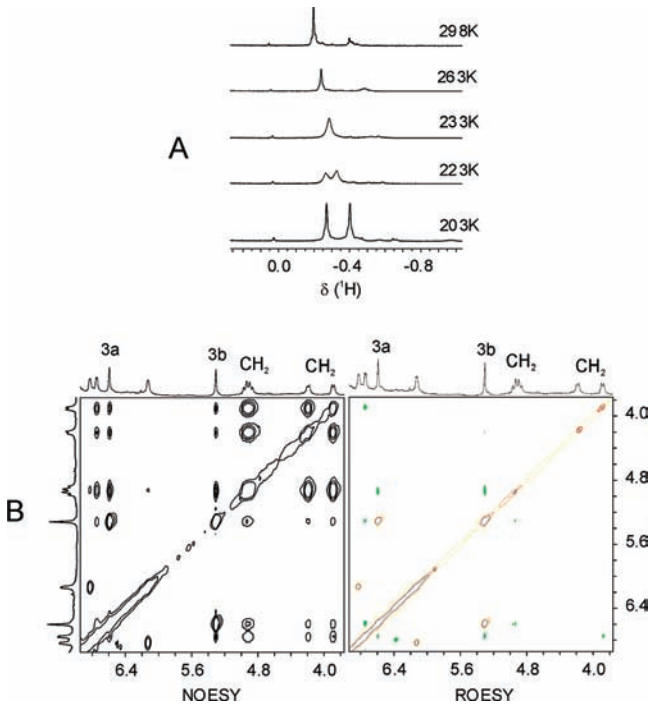

Figure 4. (A) The high-field fragments of the ^{1}H NMR spectra of **8b** taken at the temperatures specified near each trace. (B) Fragments of the NOESY and ROESY spectra recorded at 213 K for **8b**. In the ROESY map, the phase of the green cross-peaks is negative (ROE) and that of the red signals is positive (EXS).

The ^{1}H NMR spectra of the asymmetric systems **10** and **11** ($CDCl_3$, 298 K, Figure 5) unify spectral features of the appropriate 2- or 21-substituted NCP nickel(II) complexes[25,27–29] with those of the 2-alkylated ligand.[37–39] That includes signals of the "inner" protons of the "empty" macrocyclic ring, that is, 21′-CH (1.79 ppm for **10** and 1.26

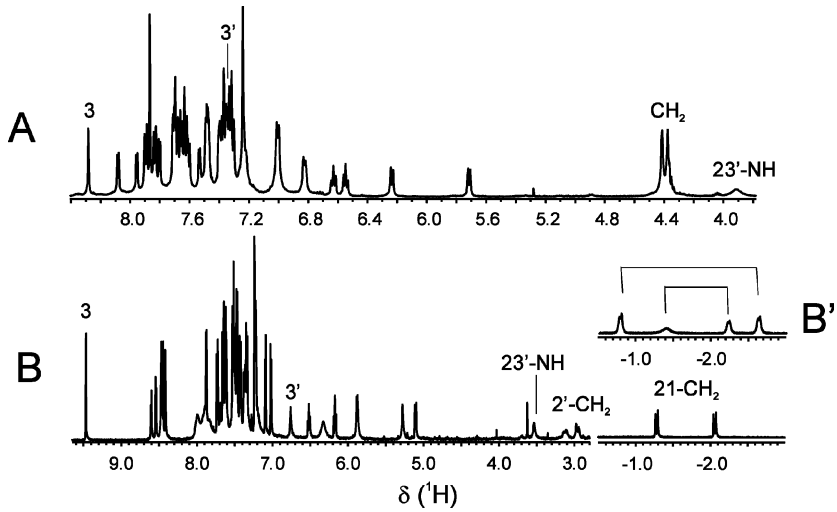

Figure 5. Fragments of the ^{1}H NMR spectra (500 MHz, $CDCl_3$) of **10** (A) and **11** (B) taken at 298 K. Inset B′ shows an upper-field part of the spectrum of **11** recorded at 213 K.

ppm for **11**), which are scalar coupled to the proton 3′ on the external carbon of the *confused* pyrrole (7.35 and 6.78 ppm), and a broader resonance of 23′-NH (3.96 and 3.55 ppm, respectively). There are two singlets of the xylene bridge CH_2 groups in the spectrum of **10**, reflecting the asymmetric character of the compound, while in the case of **11**, both methylene groups (i.e., the one that is bound to the asymmetric C21 and the other that is connected with N2′) are diastereotopic. A strong shielding effect of the aromatic ring current is reflected by a significant high-field shift of the 21-CH_2 signal and, to a lesser extent, that of 2′-CH_2, in line with the position of the 2′-xylene-NCP fragment within the inner sphere of the aromatic, nickel(II)-complexing moiety. The same effect is responsible for a high-field shift of one of the tolyllic methyl signals (1.05 ppm). The spatial proximity of this methyl group and 21-CH_2 is reflected by a correlation observed in a NOESY spectrum recorded for **11** at 298 K. At low temperatures (213 K), the spectrum of **11** alters significantly. Due to a slowing down of the rotation at the bridging xylene, each signal splits into two separate resonances, indicating the presence of rotamers that are not equally populated (40:60 from the integration of the 21-CH_2 signals, Figure 5B′).

The ^{1}H NMR spectrum of the Ni−Zn heterometallic system **12a** reveals the presence of an acetate ligand coordinated to the zinc center (Figure 6). The signal of CH_3COO^- appears at room temperature as a broad singlet shifted to 0.15 ppm (Me_{ac} in Figure 6A, 298 K, $CDCl_3$). At lower temperatures, the signal is sharpened and shifted even more upfield to −0.45 ppm (213 K, Figure 6B). The coordination of acetate, apart from the aromatic ring current affecting the chemical shift of methyl protons, is supported also by the through-space interaction of CH_3 protons with some aryl protons of the zinc-coordinated fragment observed in the NOESY map of **12a** (213 K, Figure 6B′). Analysis of the interprotonic through-space interaction reveals unfolded conformation of the dimer, similar to that observed in the case of bis-silver complex **6**. The most significant dipolar correlations are those between protons 3 or 3′, that is, protons attached to the external carbon of the *confused* pyrrole in

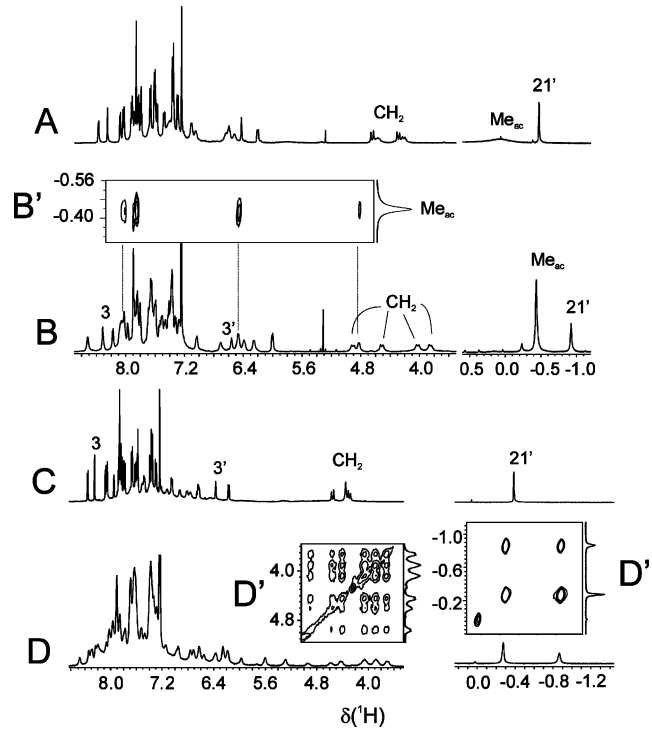

Figure 6. Fragments of the ^{1}H NMR spectra (500 MHz, $CDCl_3$) of **12a** (A, 298 K; B, 213 K) and **12b** (C, 298 K; D, 213 K). The inset B′ presents a cross-section of the NOESY map (213 K) of **12a** with correlation signals of acetate methyl protons (Me_{ac}) with *meso*-aryl protons. The insets contain fragments of the NOESY map of **12b** (213 K) presenting correlations between xylene CH_2 protons (D′) and chemical exchange signals between 21′-CH of the isomers (D″).

the nickel- or zinc-containing subunit, respectively, and methyl fragments of the tolyl substituents.

To some extent, the room-temperature ^{1}H NMR spectrum of chloride complex **12b** resembles that of **7b** superimposed on the spectrum of bis-nickel(II) complex **5**. However, only one set of signals for each fragment of the asymmetric system is observed at 298 K (Figure 7C), unlike in the case of **7b**. That reflects a fast rotation around the C−N bonds. The situation changes at lower temperatures (213 K, Figure 6D), when the spectrum reveals the presence of two nonequally populated (40:60) stereoisomers. Unlike in the cases of bis-

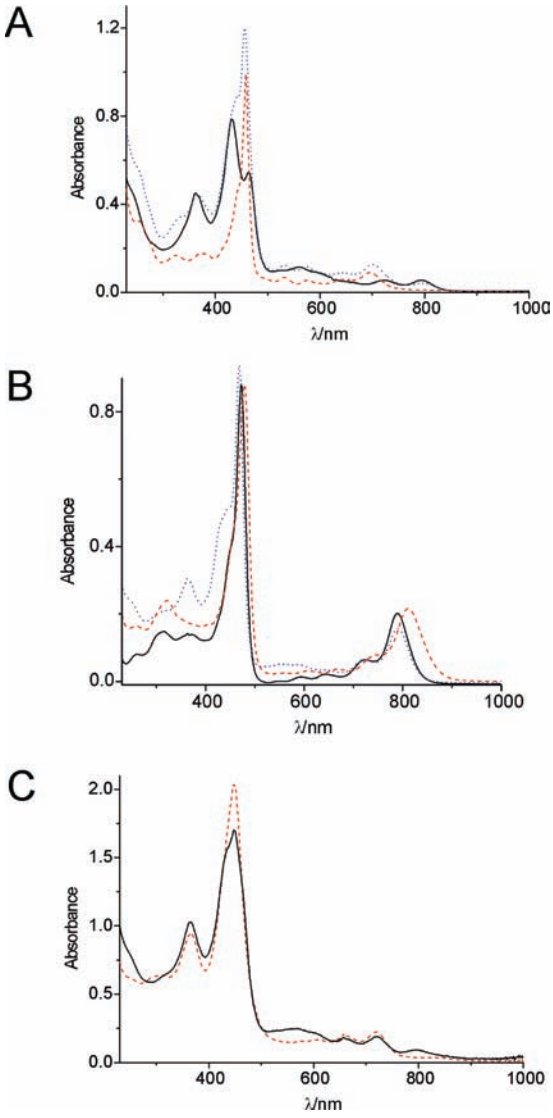

Figure 7. Optical spectra (CH_2Cl_2 solutions) of **5** (A, black solid line), **6** (A, red dashed), and **13** (A, blue doted); **7b** (B, black solid), **8a** (B, red dashed), and **12b** (B, blue doted); and **10** (C, black solid) and **11** (C, red dashed).

zinc complexes, these stereoisomers are in equilibrium, since their xylene-CH_2 or 21′-CH resonances give chemical-exchange correlation signals in the NOESY spectrum of **12b** at 213 K (Figure 6D′ and D″). It indicates a different origin of the stereoisomerism in the case of homometallic complexes **7** and **8** containing nonplanar subunits, for which differentiation is permanent, being related with a mutual orientation of apical ligands, and in the present case where the other chirality center is induced by slowing down the dynamic process. Interestingly, in the case of acetate complex **12a**, such dynamic differentiation of the signals at low temperatures does not occur. It may suggest that, due to steric factors related to the presence of the acetate ligand, the nickel-coordinated macrocyclic fragment can adopt only one orientation with respect to that of the zinc-containing moiety.

The optical properties of the homonuclear dimeric system do not seem to be significantly altered with respect to those of the monomeric complexes. It indicates lack of strong interaction between aromatic chromophores. For each of the

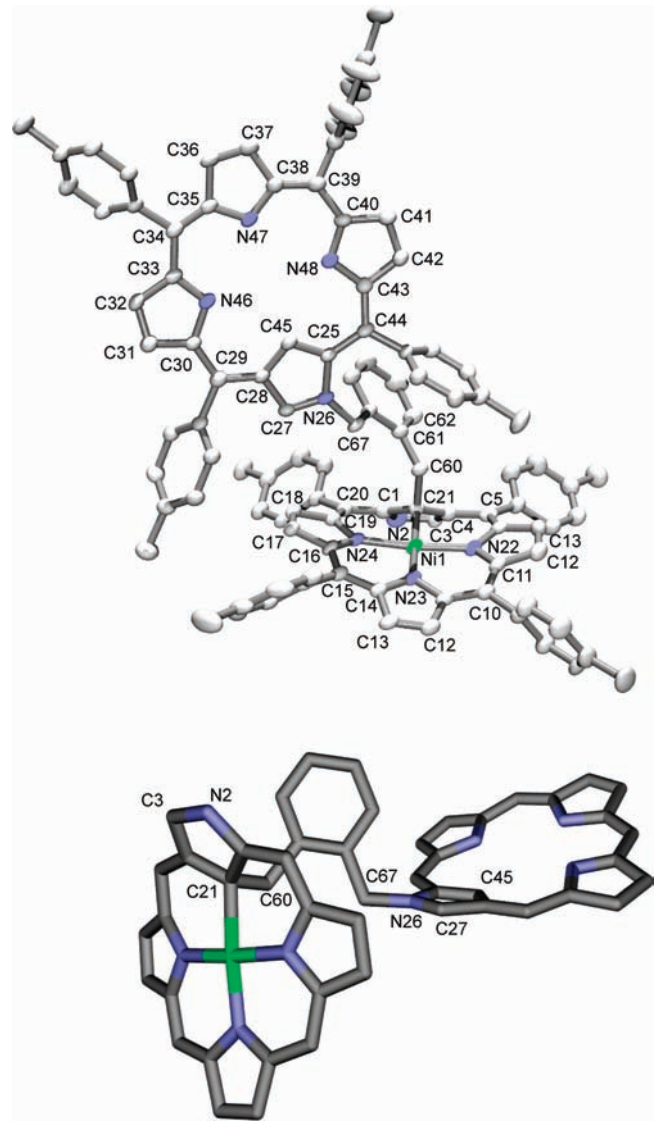

Figure 8. Top: A perspective view (with 50% thermal ellipsoids) and atom numbering scheme of **11**. All hydrogens and solvent molecules are omitted. Bottom: A wire-frame representation of the skeleton of **11** with all tolyl substituents removed. Selected bond lengths and angles: Ni1−N23, 1.963(4); Ni1−N22, 1.975(4); Ni1−N24, 1.982(4); Ni1−C21, 2.054(5); C21−C4, 1.446(7); C21−C1, 1.458(7); C21−C60; 1.582(7), C1−N2; 1.404(7); N2−C3, 1.352(7); C3−C4, 1.392(7); C45−C25, 1.392(7); C45−C28, 1.399(7); N26−C27, 1.330(7); N26−C67, 1.463(6); C27−C28, 1.418(7); N23−Ni1−N22, 92.32(17); N23−Ni1−N24, 90.67(17); N22−Ni1−N24, 174.74(16); N23−Ni1−C21, 173.11(18); N22−Ni1−C21, 87.43(18); N24−Ni1−C21, 89.09(18); C4−C21−C1, 102.0(4); C4−C21−C60, 114.7(4); C1−C21−C60, 117.8(4); C4−C21−Ni1, 118.3(3); C1−C21−Ni1, 115.8(3); C60−C21−Ni1, 89.2(3); N2−C1−C21, 109.7(4); C3−N2−C1, 108.8(5); N2−C3−C4, 108.9(4).

heterometallic complexes, the UV−vis spectrum resembles superposition of the spectra of the appropriate homodimers (Figure 7). It suggests that, although relatively close to each other and covalently bound, the subunits retain their electronic properties.

X-Ray Structure of 11. The structure of **11** in the solid state is confirmed by an X-ray diffraction analysis (Figure 8). The molecule's topology involves two subunits of the N-confused porphyrin 2′,21-linked by an *o*-xylene bridge. The macrocyclic part in the metalated subunit is slightly saddle-distorted but coordination core Ni1−C21−N22−N23−N24 is essentially planar with a 0.03 Å mean deviation

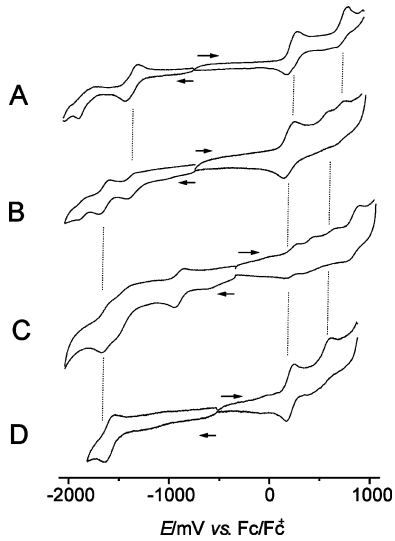

Figure 9. Cyclic voltammograms (CH_2Cl_2, 0.1 M TBAP) of homo- and heterometallic dimeric complexes: **7b** (A), **12b** (B), **13** (C), and **5** (D).

from the plane. The distances between nickel and the coordinating atoms (Ni1−C21, 2.054(5) Å; Ni1−N22, 1.975(4) Å; Ni1−N23, 1.963(4); Ni1−N24, 1.982(4)) are similar to those observed for other 21-alkylated complexes.[25,54,57] The carbon−nickel bond distance as well as a sum of the bond angles around C21 (658°) indicate σ coordination and sp^3 hybridization of this atom. Also, the ring atoms of the nonmetallated subunit do not decline significantly from planarity, and a mean deviation from the plane defined by all atoms of the macrocycle is 0.17 Å. The dihedral angle between the mean planes of the macrocyclic subunits is 112°. The orientation of the nonmetalated subunit with respect to the bridge allows a closeness of the methyl group of the tolyl substituent at C44 and methylene group C60. Such an arrangement leads to an interprotonic distance of about 2.6 Å and is consistent with the correlation between CH_2 and CH_3 protons observed in the solution NOESY experiment.

Redox Properties. Cyclovoltammetric measurements for the metal complexes of dimeric species were performed in dichloromethane using a $[BuN_4]ClO_4$ supporting electrolyte and were referenced against a ferrocene/ferrocenium internal standard. The representative electrochemical experiments are presented in Figure 9, and the data are collected in Table 1.

Due to a relatively long distance between the subunits and a lack of the coupling of the aromatic systems, no interaction of the redox centers is anticipated for homometallic 2,2′-xylene-linked bis(porphyrin) complexes **5**, **6**, and **7**. Indeed, unsplit two-electron couples are observed in the cyclic voltammograms of these complexes, indicating a simultaneous oxidation or reduction of both subunits. The irreversibility of most of the second sets of oxidations may be due to the poor solubility of the highly charged species in CH_2Cl_2,[67] although the application of a more polar solvent (THF or acetonitrile) does not significantly improve the shape of the voltammograms.

(67) Pognon, G.; Boudon, C.; Schenk, K. J.; Bach, B.; Weiss, J. *J. Am. Chem. Soc.* **2006**, *128*, 3488.

Table 1. Cyclovoltammetric Data for Homo- and Heterometallic Complexes of Xylene-Linked N-Confused bis(Porphyrins)[a]

complex	E_{ox}	$\Delta E_{ac(ox)}$	E_{red}	$\Delta E_{ac(red)}$
5	214	59	−1592	58
	595[b]	irreversible		
	942[b]	irreversible		
6	826[b]	irreversible	−867	61
			−1560	86
7b	233	80	−1357	90
	746[b]	irreversible	−1894[c]	irreversible
12b	189	85	−1373	60
	570[b]	irreversible	−1643	65
	1236	59	−1841	99
13	224	78	−889	73
	383	78	−1450	80
	644[b]	irreversible	−1532	65
	839	84		

[a] Data for dichloromethane solutions referenced with ferrocene/ferrocenium internal standard. The values (in mV) are the average of the oxidation and reduction peak potentials, unless stated otherwise. [b] Only an oxidation peak has been observed. [c] Only a reduction peak has been observed.

In the case of bis-nickel(II) adduct **5**, both first reduction and oxidation couples appear at half-wave potentials similar to those observed for monomeric complexes of NCP and its 2-N-alkylated derivatives.[9,28] In contrast to the 2,2′- or 2,21′-methylene-linked dimeric NCP nickel(II) complexes,[28,29] for which electrostatic interaction between the redox centers results in a splitting of the first oxidation couple, both subunits in **5** are oxidized at the same potential. Significantly, such electrostatic interaction, which resulted in the splitting of both oxidation and reduction waves, has been observed for isomeric system **4**, containing the same, yet differently arranged, moieties as complex **5**.[57]

Bis(chlorozinc) complex **12b** displays lower separation of the first oxidation and reduction couples than that observed in the case of **5**. It is due to a more positive potential of the first reduction wave of **12b**, while first oxidation takes place at a potential which is very similar to that observed for bis(nickel(II)) complex **5**. This similarity may suggest that, for both complexes, a ligand-centered oxidation leads to the formation of a cationic biradical species. However, the observed oxidation potential of **5** is close to those reported for the monomeric nickel(II) complexes of NCP and its 2- or 21-alkylated derivatives, for which metal-centered chemical oxidation yielded nickel(III) species, which has been shown by electron paramagnetic resonance (EPR).[25,28]

A significant alteration of redox properties with respect to that of the monomeric unsubstituted species[4] is observed for bis(silver(III)) complex **6**. A strong anodic shift of the first reduction couple ($\Delta E \sim 500$ mV) may reflect a change of the reduction site from the ligand to the metal center. It is related to the alteration of the ligand properties caused by introduction of the substituent at the external nitrogen in **6**. As a consequence of this, the macrocyclic subunits cannot fully neutralize the metal ion charge, making it prone to reduction. It is well-documented that the dianionic character of the carbaporphyrinoid ligand destabilizes trivalent metal ions with respect to the systems possessing trianionic coordination cores.[6,28,54,55,59]

In the heterometallic systems **12b** and **13**, each of the subunits containing different metals retain individual redox properties, and thus oxidation or reduction processes occur

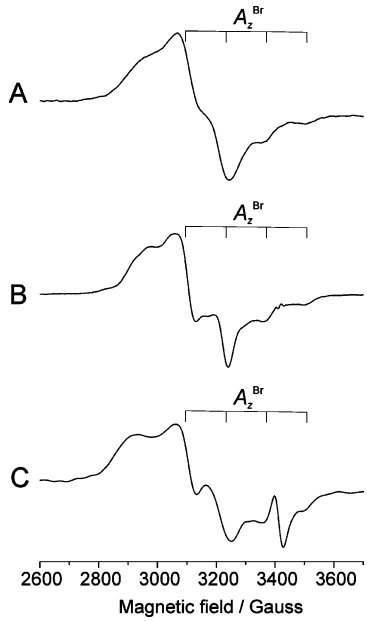

Figure 10. The frozen-solution EPR spectra of the oxidized species **5**-Br_2 (A), **12**-Br (B), and **13**-Br (C) recorded in CH_2Cl_2 at 77 K.

independently. As a result of this, their cyclic voltammograms resemble the superposition of bis(nickel(II)) complex **5** with the voltammogram of **7b** or **6**, respectively (Figure 9).

A chemical oxidation of the bis(metalated) nickel(II)-containing complexes, **5**, **12**, and **13**, with bromine can be conveniently monitored by EPR. In each case, a signal observed for the frozen solution of the oxidized species is typical for the nickel(III) complex containing one paramagnetic center with a bromide ligand coordinated to the metal ion[9,28] (Figure 10). The spin-Hamiltonian parameters ($g_x = 2.319$, $g_y = 2.186$, $g_z = 2.100$, $A_z^{Br} = 144$ G for **5**; $g_x = 2.339$, $g_y = 2.147$, $g_z = 2.103$, $A_z^{Br} = 143$ G for **12**; $g_x = 2.328$, $g_y = 2.200$, $g_z = 2.109$, $A_z^{Br} = 140$ G for **13**) are similar for all three complexes and do not vary with the concentration of the oxidizing agent. The similarity of the EPR spectral parameters between complexes containing one and two nickel(III) ions implicates a lack of magnetic interaction between the subunits in **5**-Br_2, that is, for the bis(nickel) complex in the oxidized state. This is in a sharp contrast with the case of complex **4**, for which mono- and bis-oxidized species have been detected during the titration with bromine and an interaction between the unpaired electrons has been established on the basis of spin-Hamiltonian parameters.[57]

Conclusion

The bis(N-confused porphyrin) system 2,2′-linked by *o*-xylene allows for the preparation of bis(metal) complexes, and the coordination cores retain multimodal properties typical of monomeric NCP ligands. The subunits, although relatively close to each other, do not interact. That is in contrast with the previously described system containing the same linker joining "internal" carbon atoms. Clearly, the mutual orientation of the subunits is of primary importance for their electrostatic or electronic interactions since in neither case are the π-bond systems of the subunits coupled. The closeness of the two chromophores and the semirigid character of the bridge, as well as the labile character of the complexes containing zinc or cadmium allowing facile exchange of an apical anion, make these systems suitable for application in recognition of the absolute configuration of the chiral anionic ligands by exploiting exciton coupling.[68–77] Some preliminary circular dichroism investigation of the systems containing chiral ligands gave promising results (see the Supporting Information for an example), which will be reported in due time. Also, in heterometallic complexes **12** and **13** and in mono(nickel(II)) systems **10** and **11**, the subunits' behavior seems not to be altered with respect to the monomeric complexes. The presence of two different chromophore/redox/coordination centers in one molecule is a promising feature for further application of these systems as electronic switches or photocatalysts.

Experimental Section

Instrumentation. Absorption spectra were recorded on a diode array Hewlett-Packard 8453 spectrometer. Mass spectra were recorded on a Bruker Daltonics microTOF-Q spectrometer using the electrospray technique. NMR spectra were recorded on a Bruker Avance 500 spectrometer. The 1D and 2D experiments (COSY, NOESY, heteronuclear multiple-quantum coherence (HMQC), and heteronuclear multiple-bond correlation) were performed by means of standard experimental procedures of the Bruker library. The peaks were referenced to the residual $CHCl_3$ resonances in ^1H and ^{13}C NMR (7.24 and 77.2 ppm, respectively). Cyclovoltammetric measurements were performed in dichloromethane on an EA9C MTM apparatus with a glassy carbon disk as the working electrode, Ag/AgCl as the reference electrode (the ferrocene reference potential was 530 mV), and platinum wire as the auxiliary electrode. Tetrabutylammonium perchlorate (0.1 M) was used as the supporting electrolyte. The X-band EPR spectra were obtained with a Bruker ESP 300E spectrometer. The magnetic field was calibrated with a proton magnetometer and EPR standards. Molecular modeling was performed using the HyperChem 6 Molecular Modeling System (Hypercube Inc., 2000), using the MM+ force field for the initial determination of the conformer shapes, which was followed by the PM3/RHF semiempirical energy optimization.

Caution! *The organic perchlorate salts are potentially explosive and should be handled with caution and only in small quantities.*

Syntheses of the Precursors. N-confused porphyrin **1** was synthesized by the Lindsey method.[3] Nickel complex **2** was

(68) Proni, F.; Pescitelli, G.; Huang, X.; Nakanishi, K.; Berova, N. *J. Am. Chem. Soc.* **2003**, *125*, 12914.
(69) Pescitelli, G.; Gabriel, S.; Wang, Y.; Fleischhauer, J.; Woody, R.; Berova, N. *J. Am. Chem. Soc.* **2003**, *125*, 7613.
(70) Balaz, M.; Holmes, A. E.; Banedetti, M.; Rodriguez, P. C.; Berova, N.; Nakanishi, K.; Proni, G. *J. Am. Chem. Soc.* **2005**, *127*, 4172.
(71) Huang, X.; Rickman, B. H.; Borhan, B.; Berova, N.; Nakanishi, K. *J. Am. Chem. Soc.* **1998**, *120*, 6185.
(72) Proni, G.; Pescitelli, G.; Huang, X.; Quraishi, N. Q.; Nakanishi, K.; Berova, N. *Chem. Commun.* **2002**, 1590.
(73) Borovkov, V. V.; Hembury, G. A.; Inoue, Y. *Acc. Chem. Res.* **2004**, *37*, 449.
(74) Borovkov, V. V.; Fujii, I.; Muranaka, A.; Hembury, G. A.; Tanaka, T.; Ceulemans, A.; Kobayashi, N.; Inoue, Y. *Angew. Chem., Int. Ed.* **2004**, *43*, 5481.
(75) Borovkov, V. V.; Lintuluoto, J. M.; Inoue, Y. *J. Am. Chem. Soc.* **2001**, *123*, 2979.
(76) Borovkov, V. V.; Muranaka, A.; Hembury, G. A.; Origane, Y.; Ponomarev, G. V.; Kobayashi, N.; Inoue, Y. *Org. Lett.* **2005**, *7*, 1015.
(77) Bhyrappa, P.; Borovkov, V. V.; Inoue, Y. *Org. Lett.* **2007**, *9*, 433.

obtained as described previously.[1,27,28] Xylene-containing derivatives **3** and **9** were synthesized with a method modified from one reported previously.[38] Freshly distilled THF instead of toluene as the solvent and [18]-crown-6 as a phase-transfer agent for a proton scavenger (K_2CO_3) were used in the present study. Under such conditions, a molar ratio of dimeric and monomeric products (0.6:1) is more favorable for the dimer than in the case of the formerly described method.

Synthesis of 2,2′-Bis(5,10,15,20-tetrakis(*p*-tolyl)-2-aza-21-carbaporphyrinato-nickel(II))-*o*-xylene, 5. To a solution of **3** (20 mg, 0.014 mmol) in chloroform (30 mL) was added nickel(II) acetate tetrahydrate (50 mg, 0.2 mmol) in ethanol (15 mL), and the reaction mixture was refluxed for 1 h. After that, the solvents were removed, and the complex was extracted with several 10 mL portions of dichloromethane. The extract was passed down the silica gel column with dichloromethane as an eluent. The fastest-migrating green band was collected. The solution volume was reduced to about 10 mL, and the dark green product, **5**, was precipitated with hexane. Yield: 15 mg (70%).

Selected data for **5**. UV−vis (CH_2Cl_2) λ/nm ($\epsilon \cdot 10^{-3}$): 242 sh; 626 (99.6); 431 (174.5); 463 (121.1); 526 sh; 562 (25.5); 595 (sh); 659 (sh); 725 (12.4); 796 (12.4). ^{1}H NMR (500 MHz, $CDCl_3$, 298 K): δ 8.29 (s, 1H); 8.08 (d, ^3J = 5.0 Hz, 1H); 7.87 (s, 2H); 7.83 (d, ^3J = 7.8 Hz, 2H); 7.80 (d, ^3J = 5.0 Hz, 1H); 7.68 (d, ^3J = 7.8 Hz, 2H); 7.64 (d, ^3J = 8.0 Hz, 2H); 7.62 (d, ^3J = 5.0 Hz, 1H); 7.46 (d, ^3J = 8.0 Hz, 2H); 7.44 (d, ^3J = 5.0 Hz, 1H); 7.37 (d, ^3J = 8.0 Hz, 2H); 7.32 (d, ^3J = 7.6 Hz, 2H); 7.08 (d, ^3J = 6.2 Hz, 2H); 6.94 (d, ^3J = 7.3 Hz, 2H); 6.72 (m, 1H); 6.29 (m, 1H); 4.45 (s, 2H); 2.60 (s, 3H); 2.55 (s, 3H); 2.53 (s, 3H); 2.06 (s, 3H). ^{13}C NMR (126 MHz, $CDCl_3$, 298 K): δ 154.0; 151.7; 150.9; 149.8; 148.4; 146.5; 144.6; 138.3; 137.5; 137.3; 137.1; 136.8; 136.7; 136.2; 134.7; 133.4; 133.2; 133.0; 132.9; 132.8; 132.4; 132.0; 131.4; 130.9; 130.3; 128.2; 127.8; 127.7; 127.7; 127.6; 127.4; 126.0; 124.5; 123.2; 121.2; 118.1; 117.2; 52.3; 21.4; 21.3; 20.8. MS (ESI): *m*/*z* 1556.5 (observed); 1556.2 (calculated for $C_{104}H_{76}N_8Ni_2 + H^+$).

Synthesis of 2,2′-Bis(5,10,15,20-tetrakis(*p*-tolyl)-2-aza-21-carbaporphyrinato-silver(III))-*o*-xylene Bis(tetrafluoroborate), 6. A solution containing **3** (20 mg, 0.014 mmol) and silver(I) tetrafluoroborate (15 mg, 0.08 mmol) in THF (20 mL) was stirred in darkness for 2 h at room temperature. After that, the solvent was removed, and the olive-green solution was separated from a gray precipitate (metallic silver) by extraction with benzene and filtration. The filtrate was washed with two portions of water (10 mL); the solvent was then removed, and the solid was redissolved in a minimum volume of CH_2Cl_2, and the product, **6**, was precipitated by the addition of hexane, collected by filtration, and dried in the air. Yield: 16 mg (62%).

Selected data for **6**. UV−vis (CH_2Cl_2) λ/nm ($\epsilon \cdot 10^{-3}$): 255 (77.6); 273 (sh); 327 (44.0); 379 (45.5); 416 (sh); 442 (sh); 458 (242.0); 532 (14.0); 575 (12.5); 644 (13.9); 696 (24.0). ^{1}H NMR (500 MHz, $CDCl_3$, 298 K): δ 9.14 (s, 1H); 8.81 (dd, $^3J_{HH}$ = 5.2 Hz, $^4J_{AgH}$ = 1.1 Hz, 1H); 8.51 (d, $^3J_{HH}$ = 5.0 Hz, 1H); 8.40 (d, $^3J_{HH}$ = 5.3 Hz, 1H); 8.39 (d, $^3J_{HH}$ = 5.3 Hz, 1H); 8.26 (d, $^3J_{HH}$ = 5.0 Hz, 1H); 8.18 (d, $^3J_{HH}$ = 8.0 Hz, 2H); 8.01 (dd, $^3J_{HH}$ = 5.2 Hz, $^4J_{AgH}$ = 1.1 Hz, 1H); 7.90 (d, $^3J_{HH}$ = 7.8 Hz, 2H); 7.82 (d, $^3J_{HH}$ = 8.0 Hz, 2H); 7.75 (d, $^3J_{HH}$ = 7.6 Hz, 2H); 7.56 (d, $^3J_{HH}$ = 7.6 Hz, 2H); 7.50 (d, $^3J_{HH}$ = 7.6 Hz, 2H); 6.77 (m, AA′XX′, 1H); 5.96 (m, AA′XX′, 1H); 5.49 (b, 2H); 2.73 (s, 3H); 2.67 (s, 3H); 2.63 (s, 3H); 2.09 (s, 3H). ^{13}C NMR (126 MHz, $CDCl_3$, 298 K): δ 152.4 (3-*C*H); 146.6; 145.5; 144.6; 144.5; 141.8; 139.8; 138.8; 138.7; 138.6; 136.5; 136.4; 135.1; 134.7; 134.6; 133.9; 133.7; 133.6; 133.4; 133.1; 132.9; 132.4; 132.2; 130.2; 128.9; 128.6; 128.4; 128.3; 126.5; 125.7 (d, $^1J_{AgC}$ = 57.6 Hz ^{109}Ag, $^1J_{AgC}$ = 50.0 Hz ^{107}Ag, 21-*C*); 125.0; 124.0; 122.5; 121.8; 116.0; 55.8; 21.5; 20.8. ^{11}B NMR (160.5 MHz, $CDCl_3$, 298 K): δ −1.49 (BF_4^-). HRMS (ESI+): *m*/*z* 1738.455 (observed); 1738.452 (calculated for $[C_{104}H_{78}N_8Ag_2BF_4]^+$); 826.2214 (observed); 826.2225 (calculated for $[C_{104}H_{78}N_8Ag_2]^{2+}$). Anal. calcd for $C_{104}H_{78}N_8Ag_2B_2F_8$: %C, 68.29; %H, 4.30; %N, 6.13. Observed: %C, 68.34; %H, 4.47; %N, 5.67.

Synthesis of 2,2′-Bis(5,10,15,20-tetrakis(*p*-tolyl)-2-aza-21-carbaporphyrinatozinc Chloride)-*o*-xylene, 7b. A sample of **3** (20 mg, 0.014 mmol) was dissolved in chloroform (20 mL), to which zinc acetate dihydrate solution in methanol (33 mg, 0.15 mmol in 10 mL) was added, and the mixture was stirred at room temperature for 1 h. The solvents were then removed by evaporation at room temperature, and the solid residue was dissolved in dichloromethane (15 mL) and filtered. Formation of the acetate bis(zinc) complex, **7a**, was determined by mass spectrometry (HRMS (ESI+): 1627.532 (observed); 1627.522 (calculated for $[(C_{104}H_{80}N_8Zn_2)(CH_3CO_2)]^+$). The filtrate volume was reduced to 5 mL, and the solution was vigorously stirred for 1 h with an aqueous solution of NaCl (1 M, 2 mL), after which the water layer was removed, and the organic phase was washed with three portions of water (10 mL each). After separation of the organic phase, the solution was filtered, and the solvent was removed. The solid residue was dissolved in chloroform, and the olive-green product, **7b**, was crystallized slowly after the addition of hexane. Yield: 16 mg (70%).

Selected data for **7b**. UV−vis (CH_2Cl_2) λ/nm ($\epsilon \cdot 10^{-3}$): 259 (47.9); 311 (56.2); 364 (55.7); 451 (sh); 471 (218.0); 549 (sh); 591 (13.2); 636 (17.2); 724 (20.0); 788 (53.2). ^{1}H NMR (500 MHz, $CDCl_3$, 298 K): δ 8.36 (d, $^3J_{HH}$ = 4.8 Hz, 1H$_y$); 8.24 (d, $^3J_{HH}$ = 4.6 Hz, 1H$_x$); 8.10 (d, $^3J_{HH}$ = 7.6 Hz, 2H$_y$); 8.03 (d, $^3J_{HH}$ = 4.8 Hz, 1H$_x$); 7.96 (d, $^3J_{HH}$ = 4.8 Hz, 1H$_y$); 7.88 (d, $^3J_{HH}$ = 8.2 Hz, 2H$_x$); 7.87 (d, $^3J_{HH}$ = 4.8 Hz, 1H$_y$); 7.84 (d, $^3J_{HH}$ = 4.6 Hz, 1H$_x$ + 1H$_y$); 7.82 (d, $^3J_{HH}$ = 4.8 Hz, 1H$_x$); 7.80 (d, $^3J_{HH}$ = 4.8 Hz, 1H$_x$); 7.77 (d, $^3J_{HH}$ = 4.8 Hz, 1H$_x$); 7.75 (d, $^3J_{HH}$ = 4.6 Hz, 1H$_y$); 7.74 (d, $^3J_{HH}$ = 4.6 Hz, 1H$_y$); 7.70 (b, m); 7.63 (d, $^3J_{HH}$ = 7.8 Hz, 2H$_x$); 7.53 (d, $^3J_{HH}$ = 7.1 Hz, 2H$_x$); 7.45 (d, $^3J_{HH}$ = 7.1 Hz, 2H$_y$); 7.42 (d, $^3J_{HH}$ = 7.8 Hz, 2H$_x$); 7.38 (m, 2H$_x$ + 2H$_y$); 7.04 (m, 1H$_x$); 6.94 (b, 1H$_y$); 6.81 (d, $^3J_{HH}$ = 7.8 Hz, 1H$_y$); 6.75 (m, 1H$_x$); 6.37 (s, 1H$_y$); 5.80 (s, 1H$_x$); 4.49 (d, $^2J_{HH}$ = 15.8 Hz, 1H$_x$); 4.41 (d, $^2J_{HH}$ = 17.0 Hz, 1H$_y$); 4.35 (d, $^2J_{HH}$ = 15.8 Hz, 1H$_x$); 4.08 (d, $^2J_{HH}$ = 17.0 Hz, 1H$_y$); 2.67 (s, 3H$_y$); 2.59 (s, 3H$_x$ + 3H$_y$); 2.56 (s, 6H$_x$ + 3H$_y$); 2.07 (s, 3H$_x$); 1.77 (s, 3H$_y$); −0.31 (s, 1H$_x$); −0.41 (s, 1H$_y$). ^{13}C NMR (126 MHz, $CDCl_3$, 298 K): δ 162.4; 162.2; 162.1; 161.9; 158.0; 157.8; 156.3; 156.2; 153.5; 153.4; 150.8; 150.7; 139.4; 139.2; 139.1; 138.9; 138.6; 138.5; 138.4; 138.0; 137.7; 137.4; 137.0; 136.9; 136.8; 136.6; 136.3; 136.0; 135.8; 134.3; 134.1; 133.9; 133.5; 133.4; 133.3; 133.1; 133.0; 132.3; 132.0; 131.7; 131.4; 128.7; 128.5; 128.3; 127.9; 127.8; 127.7; 127.5; 124.9; 124.5; 123.7; 122.0 (3-*C*H$_y$); 118.7 (3-*C*H$_x$); 118.4; 116.5; 116.1; 76.6 (21-*C*H$_y$); 75.0 (21-*C*H$_x$); 50.6 (*C*H$_{2x}$); 50.1 (*C*H$_{2y}$); 21.5; 21.4; 20.8; 20.8. HRMS (ESI+): 1603.473 (observed); 1603.478 (calculated for $C_{104}H_{80}N_8ClZn_2$). Anal. calcd for $C_{104}H_{80}N_8Zn_2Cl_2 \cdot H_2O \cdot$hexane: %C, 75.59; %H, 5.54; %N, 6.48. Observed: %C, 75.36; %H, 5.20; %N, 6.25.

Syntheses of 2,2′-Bis(5,10,15,20-tetrakis(*p*-tolyl)-2-aza-21-carbaporphyrinatocadmium Acetate)-*o*-xylene, 8a, and 2,2′-Bis(5,10,15,20-tetrakis(*p*-tolyl)-2-aza-21-carbaporphyrinatocadmium Chloride)-*o*-xylene, 8b. A sample of **3** (20 mg, 0.014 mmol) was dissolved in chloroform (20 mL), to which a cadmium acetate dihydrate solution in methanol (30 mg, 0.11 mmol in 10 mL) was added, and the mixture was stirred at room temperature for 1 h. The solvents were then removed by evaporation at room temperature, and the solid residue was dissolved in dichloromethane (15 mL) and filtered and washed with three 5 mL portions of water. The solvent was then removed, and the solid residue was redissolved

in a minimum amount of chloroform and precipitated by the addition of hexane. The dark-green product, **8a**, was collected by filtration and dried *in vacuo*. Yield: 20 mg (80%). A 10 mg sample of the acetate complex, **8a**, was converted into a bis(chloride) complex by dissolving it in 10 mL of chloroform and vigorous stirring with an aqueous solution of NaCl (1 M, 2 mL). The water layer was then removed, and the organic phase was washed with three portions of water (5 mL each). After separation of the organic phase, the solution was filtered, and the solvent was removed. The solid residue was dissolved in chloroform, and the product, **8b**, was crystallized slowly after the addition of hexane. Yield: 8 mg (82%).

Selected data for **8a**. UV−vis (CH_2Cl_2) λ/nm ($\epsilon \cdot 10^{-3}$): 258 (44.1); 321 (64.1); 403 (sh); 456 (sh); 478 (235.1); 560 (67.0); 608 (8.3); 669 (9.7); 739 (sh); 811 (57.8). ^{1}H NMR (500 MHz, $CDCl_3$, 298 K): δ 8.19 (d, $^3J_{HH}$ = 4.6 Hz, dd, $^3J_{HH}$ = 4.6 Hz, $^4J_{CdH}$ = 4.2 Hz, 1H$_y$); 8.13 (d, $^3J_{HH}$ = 4.8 Hz, dd, $^3J_{HH}$ = 4.8 Hz, $^4J_{CdH}$ = 4.4 Hz, 1H$_x$); 7.96 (d, $^3J_{HH}$ = 7.9 Hz, 2H$_y$); 7.90 (d, $^3J_{HH}$ = 4.8 Hz, 1H$_x$); 7.90 (d, $^3J_{HH}$ = 7.6 Hz, 1H$_x$); 7.85 (d, $^3J_{HH}$ = 5.0 Hz, 1H$_y$); 7.84 (d, $^3J_{HH}$ = 4.6 Hz, 1H$_y$); 7.83 (d, $^3J_{HH}$ = 4.8 Hz, 1H$_y$); 7.82 (d, $^3J_{HH}$ = 4.2 Hz, 1H$_x$); 7.81 (d, $^3J_{HH}$ = 4.2 Hz, 1H$_x$); 7.72 (d, $^3J_{HH}$ = 4.6 Hz, dd, $^3J_{HH}$ = 4.6 Hz, $^4J_{CdH}$ = 4.3 Hz, 1H$_y$); 7.69 (b, 1H$_y$); 7.66 (d, $^3J_{HH}$ = 5.0 Hz, dd, $^3J_{HH}$ = 5.0 Hz, $^4J_{CdH}$ = 3.6 Hz, 1H$_y$); 7.65 (d, $^3J_{HH}$ = 4.8 Hz, dd, $^3J_{HH}$ = 4.8 Hz, $^4J_{CdH}$ = 4.4 Hz, 2H$_x$); 7.61 (b, 1H$_y$); 7.57 (d, $^3J_{HH}$ = 7.1 Hz, 1H$_x$); 7.55 (d, $^3J_{HH}$ = 7.3 Hz, 1H$_x$); 7.44 (d, $^3J_{HH}$ = 7.6 Hz, 2H$_x$); 7.41 (d, $^3J_{HH}$ = 7.9 Hz, 1H$_y$); 7.36 (m, 2H$_x$ + 2H$_y$); 7.11 (m, 1H$_x$); 7.02 (b, 2H$_y$); 6.96 (d, $^3J_{HH}$ = 7.3 Hz, 1H$_x$); 6.79 (m, 1H$_y$); 6.49 (m, 1H$_y$); 6.41 (d, $^4J_{HH}$ = 1.5 Hz, 1H$_y$); 6.02 (b, 1H$_x$); 4.83 (d, $^2J_{HH}$ = 16.2 Hz, 1H$_x$); 4.68; 4.53 (d, $^2J_{HH}$ = 16.2 Hz, 1H$_x$); 4.32 (d, $^2J_{HH}$ = 16.5 Hz, 1H$_y$); 2.56 (s, 3H$_x$ + 6H$_y$); 2.55 (s, 6H$_x$ + 6H$_y$); 2.51 (s, 3H$_y$); 2.09 (s, 3H$_x$); 1.12 (s, 3H$_x$ + 3H$_y$, acetate); −0.47 (d, $^4J_{HH}$ = 1.4 Hz, dd, $^4J_{HH}$ = 1.4 Hz, $^2J_{CdH}$ = 12.0 Hz, 1H$_x$); −0.54 (d, $^4J_{HH}$ = 1.5 Hz, dd, $^4J_{HH}$ = 1.5 Hz, $^2J_{CdH}$ = 12.2 Hz, 1H$_y$). ^{13}C NMR (126 MHz, $CDCl_3$, 298 K): δ 176.6; 163.3; 162.9; 160.2; 158.3; 154.3; 151.3; 139.2; 139.1; 138.7; 138.4; 137.8; 136.9; 136.7; 136.7; 136.4; 135.8; 134.9; 134.1; 134.1; 133.4; 133.0; 132.8; 132.2; 131.9; 131.4; 131.3; 130.9; 130.7; 129.0; 128.8; 128.9; 128.7; 128.6; 128.5; 128.4; 127.7; 127.6; 126.4; 126.2; 125.9; 122.7; 122.2 (*C*3$_y$); 119.7 (*C*3$_x$); 117.5; 75.3 (C21$_y$); 73.0 (*C*21$_x$); 51.0; 50.8; 29.7; 21.4; 21.4; 20.8; 21.0; 20.5. MS (ESI+): 1726.1 (observed); 1725.7 (calculated for $[(C_{104}H_{80}N_8Cd_2)(CH_3CO_2)]^+$); 833.0 (observed); 833.3 (calculated for $[C_{104}H_{80}N_8Cd_2]^{2+}$). Anal. calcd for $C_{108}H_{86}N_8Cd_2O_4 \cdot CHCl_3$: %C, 68.76; % H, 4.61; %N, 5.88. Observed: %C, 68.81; %H, 4.97; %N, 5.50.

Selected data for **8b**. UV−vis (CH_2Cl_2) λ/nm ($\epsilon \cdot 10^{-3}$): 321 (62.5); 362 (sh); 405 (sh); 433 (sh); 455 (sh); 478 (238.0); 560 (73.8); 605 (8.8); 667 (9.8); 743 (21.6); 807 (21.8). ^{1}H NMR (500 MHz, $CDCl_3$, 298 K): δ 8.25 (d, $^3J_{HH}$ = 4.6 Hz, dd, $^3J_{HH}$ = 4.6 Hz, $^4J_{CdH}$ = 4.1 Hz, 1H$_y$); 8.13 (d, $^3J_{HH}$ = 4.4 Hz, dd, $^3J_{HH}$ = 4.4 Hz, $^4J_{CdH}$ = 4.3 Hz, 1H$_x$); 8.08 (d, $^3J_{HH}$ = 8.0 Hz, 2H$_y$); 7.95 (d, $^3J_{HH}$ = 4.8 Hz, dd, $^3J_{HH}$ = 4.8 Hz, $^4J_{CdH}$ = 4.9 Hz, 1H$_x$); 7.90 (d, $^3J_{HH}$ = 7.6 Hz, 2H$_x$); 7.87 (d, $^3J_{HH}$ = 5.0 Hz, 1H$_y$); 7.85 (d, $^3J_{HH}$ = 5.0 Hz, 1H$_y$); 7.84 (d, $^3J_{HH}$ = 4.6 Hz, 1H$_y$); 7.80 (s, 2H$_x$); 7.73 (d, $^3J_{HH}$ = 4.6 Hz, 1H$_y$); 7.68 (b, 2H$_x$); 7.65 (d, $^3J_{HH}$ = 4.6 Hz, dd, $^3J_{HH}$ = 4.6 Hz, $^4J_{CdH}$ = 4.7 Hz, 1H$_x$); 7.64 (d, $^3J_{HH}$ = 4.6 Hz, 1H$_y$); 7.60 (d, $^3J_{HH}$ = 4.6 Hz, 1H$_x$); 7.54 (b, 2H$_y$); 7.45 (m, 1H$_y$ + 2H$_x$); 7.38 (m, 2H$_y$ + 2H$_x$); 7.20 (b, 1H$_y$); 7.16 (b, 1H$_x$); 7.01 (b, 2H$_y$); 6.82 (d, $^3J_{HH}$ = 7.3 Hz, 1H$_x$); 6.50 (d, $^4J_{HH}$ = 1.2 Hz, 1H$_y$); 5.88 (b, 1H$_x$); 4.69 (d, $^2J_{HH}$ = 16.2 Hz, 1H$_x$); 4.52 (d, $^2J_{HH}$ = 17.4 Hz, 1H$_y$); 4.45 (d, $^2J_{HH}$ = 15.2 Hz, 1H$_x$); 4.24 (d, $^2J_{HH}$ = 17.0 Hz, 1H$_y$); 2.67 (s, 3H$_y$); 2.57 (s, 3H$_x$ + 6H$_y$); 2.55 (s, 3H$_x$); 2.53 (s, 3H$_x$); 2.00 (s, 3H$_x$); 1.84 (s, 3H$_y$); −0.20 (d, $^4J_{HH}$ = 1.4 Hz, dd, $^4J_{HH}$ = 1.4 Hz, $^2J_{CdH}$ = 12.1 Hz, 1H$_x$); −0.40 (d, $^4J_{HH}$ = 1.2 Hz, dd, $^4J_{HH}$ = 1.2 Hz, $^2J_{CdH}$ = 11.5 Hz, 1H$_y$).

Synthesis of 2-(2′-(5,10,15,20-Tetrakis(*p*-tolyl)-2-aza-21-carbaporphyrinatonickel(II))-*o*-xylene)-(5,10,15,20-tetrakis(*p*-tolyl)-2-aza-21-carbaporphyrin, 10, and 2-(21′-(5,10,15,20-Tetrakis(*p*-tolyl)-2-aza-21-carbaporphyrinatonickel(II))-*o*-xylene)-5,10,15,20-tetrakis(*p*-tolyl)-2-aza-21-carbaporphyrin, 11. To a solution containing **2** (25 mg, 0.07 mmol) and **9** (32 mg, 0.07 mmol) in THF (20 mL) was added 10 mg of K_2CO_3 and 2 mg of [18]-crown-6, and the mixture was stirred and refluxed under nitrogen for 3 h. After that, the solution was filtered, the solvent was evaporated, and the solid residue was dissolved in CH_2Cl_2. The solution was passed down a silica-gel column with dichloromethane or a 1% solution of ethanol in chloroform as the mobile phase. The fastest-migrating band contained a small amount of unreacted **2**; the second band contained product **10**, and the third contained product **11**. Solvents from the fractions containing the desired products were evaporated, dissolved in chloroform, and precipitated with hexane. The green product, **10**, and brown product, **11**, were separated from the solution by filtration and dried in the air. Yields: **10**, 25 mg (47%); **11**, 11 mg (20%).

Selected data for **10**. UV−vis (CH_2Cl_2) λ/nm ($\epsilon \cdot 10^{-3}$): 253 (sh); 309 (sh); 364 (60.5); 433 (sh); 449 (100.0); 567 (14.6); 661 (10.1); 721 (11.2); 796 (5.4). ^{1}H NMR (500 MHz, $CDCl_3$, 298 K): δ 8.28 (s, 1H); 8.08 (d, $^3J_{HH}$ = 5.0 Hz, 1H); 7.95 (d, $^3J_{HH}$ = 4.8 Hz, 1H); 7.89 (d, $^3J_{HH}$ = 7.8 Hz, 2H); 7.86 (s, 2H); 7.83 (d, $^3J_{HH}$ = 7.8 Hz, 2H); 7.80 (d, $^3J_{HH}$ = 5.0 Hz, 1H); 7.71 (d, $^3J_{HH}$ = 4.4 Hz, 1H); 7.70 (d, $^3J_{HH}$ = 5.0 Hz, 1H); 7.69 (d, $^3J_{HH}$ = 5.0 Hz, 1H); 7.67 (d, $^3J_{HH}$ = 7.8 Hz, 2H); 7.64 (d, $^3J_{HH}$ = 8.0 Hz, 2H); 7.62 (d, $^3J_{HH}$ = 7.8 Hz, 2H); 7.60 (d, $^3J_{HH}$ = 5.0 Hz, 1H); 7.53 (d, $^3J_{HH}$ = 4.6 Hz, 1H); 7.49 (d, $^3J_{HH}$ = 7.8 Hz, 2H); 7.47 (d, $^3J_{HH}$ = 7.8 Hz, 2H); 7.40 (d, $^3J_{HH}$ = 4.6 Hz, 1H); 7.39 (d, $^3J_{HH}$ = 5.0 Hz, 1H); 7.38 (d, $^3J_{HH}$ = 7.8 Hz, 2H); 7.36 (d, $^3J_{HH}$ = 7.8 Hz, 2H); 7.35 (d, $^4J_{HH}$ = 1.4 Hz, 1H); 7.34 (d, $^3J_{HH}$ = 7.1 Hz, 2H); 7.32 (d, $^3J_{HH}$ = 7.4 Hz, 2H); 7.31 (d, $^3J_{HH}$ = 8.0 Hz, 2H); 7.00 (d, $^3J_{HH}$ = 7.4 Hz, 2H); 6.82 (d, $^3J_{HH}$ = 7.3 Hz, 1H); 6.63 (t, $^3J_{HH}$ = 7.4 Hz, 1H); 6.5 (t, $^3J_{HH}$ = 7.6 Hz, 1H); 6.23 (d, $^3J_{HH}$ = 7.6 Hz, 1H); 5.71 (d, $^3J_{HH}$ = 7.8 Hz, 1H); 4.41 (s, 2H); 4.37 (s, 2H); 3.91 (b, 1H); 2.61 (s, 3H); 2.55 (s, 3H); 2.52 (s, 3H); 2.51 (s, 3H); 2.12 (s, 3H); 1.99 (s, 3H); 1.81 (d, $^4J_{HH}$ = 1.4 Hz, 1H). ^{13}C NMR (126 MHz, $CDCl_3$, 298 K): δ 163.5; 149.9; 148.6; 144.7; 144.5; 138.7; 138.6; 138.0; 137.7; 137.4; 137.0; 136.9; 135.3; 135.2; 135.1; 134.7; 133.5; 133.0; 132.9; 132.6; 130.9; 128.1; 127.9; 127.7; 127.4; 126.0; 124.6; 121.2; 117.3; 117.0; 115.8; 115.7; 115.6; 115.5; 114.6; 114.5; 114.4; 114.3; 114.2; 113.8; 113.3; 113.1; 112.9; 112.6; 112.0; 111.2; 111.1; 111.0; 110.9; 110.8; 110.6; 108.6; 98.4 (*C*21); 60.5; 60.0; 40.2; 39.8. HRMS (ESI+): *m*/*z* 1499.599 (observed); 1499.594 (calculated for $[C_{104}H_{81}N_8Ni]^+$, $[M+1]^+$). Anal. calcd for $C_{104}H_{80}N_8Ni \cdot CHCl_3 \cdot$hexane: %C, 78.14; %H, 5.61; %N, 6.57. Observed: %C, 78.50; %H, 5.38; %N, 6.64.

Selected data for **11**. UV−vis (CH_2Cl_2) λ/nm ($\epsilon \cdot 10^{-3}$): 251 (sh); 303 (49.2); 365 (71.3); 447 (155.2); 580 (12.0); 609 (12.8); 662 (15.3); 719 (17.2); 877 (sh). ^{1}H NMR (500 MHz, $CDCl_3$, 298 K): δ 9.47 (s, 1H); 8.61 (d, $^3J_{HH}$ = 4.6 Hz, 1H); 8.55 (d, $^3J_{HH}$ = 5.1 Hz, 1H); 8.49 (d, $^3J_{HH}$ = 4.2 Hz, 1H); 8.47 (d, $^3J_{HH}$ = 4.2 Hz, 1H); 8.46 (d, $^3J_{HH}$ = 4.8 Hz, 1H); 8.42 (d, $^3J_{HH}$ = 4.6 Hz, 1H); 8.00 (b, 2H); 7.90 (d, $^3J_{HH}$ = 4.6 Hz, 1H); 7.88 (d, $^3J_{HH}$ = 4.6 Hz, 2H); 7.83 (b, 1H); 7.79 (d, $^3J_{HH}$ = 8.0 Hz, 1H); 7.73 (d, $^3J_{HH}$ = 8.0 Hz, 2H); 7.69 (d, $^3J_{HH}$ = 8.0 Hz, 1H); 7.68 (d, $^3J_{HH}$ = 4.3 Hz, 1H); 7.66 (d, $^3J_{HH}$ = 8.0 Hz, 2H); 7.65 (d, $^3J_{HH}$ = 5.0 Hz, 1H); 7.62 (d, $^3J_{HH}$ = 5.0 Hz, 1H); 7.53 (d, $^3J_{HH}$ = 7.8 Hz, 2H); 7.47 (d, $^3J_{HH}$ = 7.8 Hz, 2H); 7.43 (d, $^3J_{HH}$ = 7.8 Hz, 2H); 7.42 (d, $^3J_{HH}$ = 8.0 Hz, 1H); 7.38 (d, $^4J_{HH}$ = 1.4 Hz, 1H); 7.36 (d, $^3J_{HH}$ = 8.0 Hz,

Table 2. Crystal Data and Structure Refinement for **11** $(H_2O)(n\text{-Heptane})$

empirical formula	$C_{118}H_{113}N_8NiO$
fw	1717.87
temp	100(2) K
wavelength	1.54178 Å
cryst syst	triclinic
space group	$P\bar{1}$
unit cell dimensions	
a	17.007(3) Å
b	18.130(3) Å
c	18.797(2) Å
α	105.856(13)°
β	107.447(13)°
γ	98.818(15)°
V	5141.1(15) Å^3
Z	2
density (calcd) 1.114 Mg/m^3	
abs coeff (Cu Kα)	0.666 mm^{-1}
$F(000)$	1826
cryst size	0.3 × 0.2 × 0.15 mm^3
cryst color and habit	black prism
diffractometer	Oxford Diffraction Xcalibur PX
θ range for data collection	4.15−60.0°
index ranges	$-14 < h < 19$, $-19 < k < 18$, $-21 < l < 21$
reflns collected	39 282
ind reflns (R_{int})	14 517 (0.046)
solution method	direct
refinement method	full-matrix least-squares on F^2
data/restraints/params	14517/66/1181
GOF on F^2	1.071
final R indices [$I > 2\sigma(I)$][a]	R1 = 0.0980, wR2 = 0.2682
R indices (all data)[a]	R1 = 0.1266, wR2 = 0.2845
largest diff peak and hole	1.71 and −0.37 e Å^{-3}

[a] $R1 = \sum||F_o| - |F_c||/\sum|F_o|$, $wR2 = [\sum[w(F_o^2 - F_c^2)^2/\sum[w(F_o^2)^2]]^{1/2}$.

1H); 7.34 (d, $^3J_{HH}$ = 7.8 Hz, 2H); 7.10 (d, $^3J_{HH}$ = 4.8 Hz, 1H); 7.03 (d, $^3J_{HH}$ = 4.8 Hz, 1H); 6.52 (t, $^3J_{HH}$ = 7.6 Hz, 1H); 6.33 (b, 1H); 6.17 (t, $^3J_{HH}$ = 7.6 Hz, 1H); 5.89 (d, $^3J_{HH}$ = 6.8 Hz, 1H); 5.28 (b, 1H); 5.10 (d, $^3J_{HH}$ = 7.8 Hz, 1H); 3.53 (b, 1H); 3.14 (d, $^2J_{HH}$ = 17.1 Hz, 1H); (d, $^2J_{HH}$ = 17.2 Hz, 1H); 2.96 (s, 3H); 2.69 (s, 3H); 2.66 (s, 3H); 2.65 (s, 3H); 2.58 (s, 3H); 2.57 (s, 3H); 2.54 (s, 3H); 2.45 (s, 3H); 1.26 (d, $^4J_{HH}$ = 1.4 Hz, 1H); 1.03 (s, 3H); −1.28 (d, $^2J_{HH}$ = 14.7 Hz, 1H); −2.06 (d, $^2J_{HH}$ = 14.7 Hz, 1H). ^{13}C NMR (126 MHz, $CDCl_3$, 298 K): δ 178.7; 163.0; 157.3 (*C*3′); 156.4; 154.1; 153.9; 153.7; 153.1; 150.0; 149.3; 147.8; 147.1; 143.4; 143.2; 138.8; 138.7; 138.7; 138.3; 138.2; 138.0; 137.9; 137.6; 137.4; 137.3; 137.0 (*C*3); 136.7; 136.6; 136.5; 135.9; 135.5; 135.4; 134.9; 134.9; 134.7; 134.6; 134.1; 133.8; 133.7; 133.4; 133.3; 133.0; 132.5; 132.3; 132.2; 131.6; 131.2; 130.7; 130.4; 130.4; 130.0; 129.4; 129.1; 128.9; 128.7; 128.5; 128.1; 128.0; 127.9; 127.8; 127.5; 127.1; 126.6; 126.3; 126.1; 125.7; 125.3; 124.3; 123.8; 123.6; 115.4; 115.1; 108.5 (*C*21); 108.2; 50.3; 30.7 (*C*21′); 21.6; 21.4; 21.3; 20.0. HRMS (ESI+): *m*/*z* 1499.585 (observed); 1499.594 (calculated for $[C_{104}H_{81}N_8Ni]^+$, $[M+1]^+$).

X-Ray Data Collection and Refinement of 11. Crystals of **11**·(H_2O)(*n*-heptane) were prepared by the diffusion of *n*-heptane into the dichloromethane solution contained in a thin tube. Data were collected at 100 K using an Oxford Cryosystem device on an Oxford Diffraction Xcalibur PX diffractometer with a KM4CCD Sapphire detector. Data collection, integration, and scaling of the reflections were performed by means of the CrysAlis suite of programs (Oxford Diffraction, Poland). Crystal data are compiled in Table 2. The structure was solved by direct methods with SHELXS97[78] and refined by the full-matrix least-squares method on all F^2 data using the SHELXL97[79] programs. All non-H atoms were refined with anisotropic displacement parameters, except for those in the region of the disordered solvents; hydrogen atoms were included from the geometry of molecule. The asymmetric unit contains one molecule of **11**, two disordered molecules of *n*-heptane (in four sites), and a molecule of water disordered into four sites. A 2-fold disorder of the N-confused pyrrole of metalated subunits of **11** was treated by the assignment of half of the nitrogen and half of the carbon atoms to both C3 and N2 sites.

Synthesis of 2-(2′-(5,10,15,20-Tetrakis(*p*-tolyl)-2-aza-21-carbaporphyrinatonickel(II))-*o*-xylene)-(5,10,15,20-tetrakis(*p*-tolyl)-2-aza-21-carbaporphyrinatozinc) acetate, 12a, and 2-(2′-(5,10,15,20-Tetrakis(*p*-tolyl)-2-aza-21-carbaporphyrinatonickel(II))-*o*-xylene)-(5,10,15,20-tetrakis(*p*-tolyl)-2-aza-21-carbaporphyrinatozinc) chloride, 12b. A sample of **10** (10 mg, 0.007 mmol) was dissolved in dichloromethane (10 mL), to which a zinc acetate dihydrate solution in methanol (10 mg, 0.05 mmol in 10 mL) was added, and the mixture was stirred at room temperature for 1 h. The solvents were then removed by evaporation, and the solid residue was dissolved in dichloromethane (15 mL) and filtered. The filtrate volume was reduced to 5 mL, and hexane was added, causing the precipitation of a brown solid product, **12a**, that was collected by filtration and dried in the air. Yield: 10 mg (88%). Conversion into chloride complex **12b** was done by dissolution of **12a** (10 mg) in dichloromethane (10 mL) and vigorous stirring for 1 h with an aqueous solution of NaCl (1 M, 2 mL). The water layer was then removed, and the organic phase was washed with three portions of water (10 mL each). After separation of the organic phase, the solution was filtered, and the solvent was removed. The solid residue was dissolved in chloroform, and the dark green product, **12b**, was crystallized by the addition of hexane. Yield: 9 mg (91%).

Selected data for **12a**. UV−vis (CH_2Cl_2) λ/nm ($\epsilon \cdot 10^{-3}$): 252 (sh); 311 (sh); 363 (64.2); 433 (sh); 443 (sh); 468 (194.2); 556 (12.9); 589 (11.0); 644 (sh); 723 (20.0); 790 (34.2). ^{1}H NMR (500 MHz, $CDCl_3$, 298 K): δ 8.37 (d, $^3J_{HH}$ = 4.8 Hz, 1H); 8.25 (s, 1H); 8.08 (d, $^3J_{HH}$ = 5.0 Hz, 1H); 8.03 (d, $^3J_{HH}$ = 7.8 Hz, 2H); 7.93 (d, $^3J_{HH}$ = 5.0 Hz, 1H); 7.90 (d, $^3J_{HH}$ = 5.0 Hz, 2H); 7.88 (d, $^3J_{HH}$ = 4.8 Hz, 1H); 7.86 (s, 2H); 7.83 (d, $^3J_{HH}$ = 8.0 Hz, 2H); 7.80 (d, $^3J_{HH}$ = 4.8 Hz, 1H); 7.79 (d, $^3J_{HH}$ = 4.8 Hz, 1H); 7.68 (b, 1H); 7.66 (d, $^3J_{HH}$ = 7.6 Hz, 2H); 7.61 (d, $^3J_{HH}$ = 7.6 Hz, 3H); 7.57 (d, $^3J_{HH}$ = 5.0 Hz, 1H); 7.48 (d, $^3J_{HH}$ = 7.1 Hz, 1H); 7.40 (b, 2H); 7.36 (d, $^3J_{HH}$ = 7.8 Hz, 2H); 7.34 (d, $^3J_{HH}$ = 4.9 Hz, 1H); 7.29 (d, $^3J_{HH}$ = 7.6 Hz, 2H); 7.10 (d, $^3J_{HH}$ = 6.2 Hz, 2H); 7.05 (b, 1H); 6.63 (b, 1H); 6.59 (t, $^3J_{HH}$ = 7.0 Hz, 1H); 6.52 (b, 1H); 6.43 (s, 1H); 6.20 (d, $^3J_{HH}$ = 8.0 Hz, 1H); 4.65 (d, $^2J_{HH}$ = 17.4 Hz, 1H); 4.57 (b, 1H); 4.29 (d, $^2J_{HH}$ = 16.7 Hz, 1H); 4.21 (d, $^2J_{HH}$ = 16.4 Hz, 1H); 2.66 (s, 3H); 2.62 (s, 3H); 2.58 (s, 3H); 2.55 (s, 6H); 2.50 (s, 3H); 2.14 (s, 3H); 1.97 (s, 3H); 0.09 (b, 3H); −0.47 (s, 1H).

Selected data for **12b**. UV−vis (CH_2Cl_2) λ/nm ($\epsilon \cdot 10^{-3}$): 251 (sh); 365 (79.3); 439 (111.0); 468 (182.6); 559 (18.8); 586 (19.8); 629 (19.2); 722 (16.5); 792 (33.6). ^{1}H NMR (500 MHz, $CDCl_3$, 298 K): δ 8.36 (d, $^3J_{HH}$ = 4.8 Hz, 1H); 8.25 (s, 1H); 8.08 (d, $^3J_{HH}$ = 5.0 Hz, 1H); 8.06 (d, $^3J_{HH}$ = 8.0 Hz, 2H); 7.95 (d, $^3J_{HH}$ = 5.0 Hz, 1H); 7.88 (d, $^3J_{HH}$ = 4.8 Hz, 1H); 7.87 (d, $^3J_{HH}$ = 4.8 Hz, 1H); 7.86 (s, 2H); 7.85 (d, $^3J_{HH}$ = 5.0 Hz, 1H); 7.83 (d, $^3J_{HH}$ = 7.6 Hz, 2H); 7.80 (d, $^3J_{HH}$ = 5.0 Hz, 1H); 7.78 (d, $^3J_{HH}$ = 5.0 Hz, 1H); 7.67 (d, $^3J_{HH}$ = 8.0 Hz, 2H); 7.61 (d, $^3J_{HH}$ = 7.8 Hz, 2H); 7.59 (d, $^3J_{HH}$ = 7.8 Hz, 2H); 7.58 (d, $^3J_{HH}$ = 5.0 Hz, 1H); 7.51 (d, $^3J_{HH}$ = 7.6 Hz, 1H); 7.48 (d, $^3J_{HH}$ = 7.6 Hz, 1H); 7.39 (d, $^3J_{HH}$ =

(78) Sheldrick, G. M. *SHELXS97 - Program for Crystal Structure Solution*; University of Göttingen: Göttingen, Germany, 1997.

(79) Sheldrick, G. M. *SHELXL97 - Program for Crystal Structure Refinement*; University of Göttingen: Göttingen, Germany , 1997.

5.0 Hz, 1H); 7.36 (d, $^3J_{HH}$ = 7.8 Hz, 3H); 7.30 (d, $^3J_{HH}$ = 8.0 Hz, 2H); 7.13 (d, $^3J_{HH}$ = 8.3 Hz, 1H); 7.05 (d, $^3J_{HH}$ = 7.5 Hz, 2H); 6.93 (d, $^3J_{HH}$ = 7.3 Hz, 1H); 6.81 (d, $^3J_{HH}$ = 7.6 Hz, 1H); 6.76 (t, $^3J_{HH}$ = 7.0 Hz, 1H); 6.65 (d, $^3J_{HH}$ = 7.6 Hz, 1H); 6.63 (d, $^3J_{HH}$ = 6.5 Hz, 1H); 6.46 (b, 1H); 6.37 (s, 1H); 6.17 (d, $^3J_{HH}$ = 7.6 Hz, 1H); 4.56 (d, $^2J_{HH}$ = 17.0 Hz, 1H); 4.35 (s, 2H); 4.29 (d, $^2J_{HH}$ = 17.0 Hz, 1H); 2.65 (s, 3H); 2.62 (s, 3H); 2.58 (s, 3H); 2.55 (s, 6H); 2.50 (s, 3H); 2.07 (s, 3H); 1.95 (s, 3H); −0.38 (d, $^4J_{HH}$ = 1.4 Hz, 1H). ^{13}C NMR (126 MHz, $CDCl_3$, 298 K): δ 162.6; 162.2; 158.2; 156.6; 154.3; 153.9; 152.0; 151.3; 151.1; 150.1; 151.3 (*C*3); 148.7; 146.8; 145.0; 139.7; 139.0; 138.9; 138.8; 138.7; 138.1; 137.8; 137.6; 137.5; 137.4; 137.3; 137.2; 137.2; 137.1; 136.8; 136.3; 134.9; 134.7; 134.4; 134.3; 134.0; 133.8; 133.7; 133.5; 133.4; 133.2; 132.7; 132.4; 132.3; 132.2; 131.7; 131.5; 131.2; 130.6; 130.4; 128.7; 128.5; 128.3; 128.2; 128.0; 127.9; 127.6; 126.3; 125.9; 124.6; 123.8; 123.7; 122.6 (*C*3′); 121.5; 119.3; 118.5; 117.5; 116.9; 79.0 (*C*21′); 52.5; 51.3; 21.9; 21.8; 21.3; 21.2. HRMS (ESI+): *m*/*z* 1593.500 (observed); 1593.497 (calculated for $[C_{104}H_{79}N_8NiZn]^+$, $[M\text{-}Cl]^+$).

Synthesis of 2-(2′-(5,10,15,20-Tetrakis(*p*-tolyl)-2-aza-21-carbaporphyrinatonickel(II))-*o*-xylene)-(5,10,15,20-tetrakis(*p*-tolyl)-2-aza-21-carbaporphyrinatosilver(III)) Tetrafluoroborate, 13. A sample of **10** (10 mg, 0.007 mmol) and silver(I) tetrafluoroborate (5 mg, 0.03 mmol) was dissolved in THF (10 mL) and stirred in darkness for 2 h at room temperature. The solvent was then removed, and the olive-green product was dissolved in dichloromethane and filtered. The filtrate was washed with two portions of water (5 mL); the solvent was then removed, and the solid was redissolved in a minimum volume of CH_2Cl_2 and precipitated by the addition of hexane, collected by filtration, and dried in the air. Yield: 8 mg (67%).

Selected data for **13**. UV−vis (CH_2Cl_2) λ/nm ($\epsilon \cdot 10^{-3}$): 253 (sh); 332 (sh); 367 (75.2); 433 (sh); 441 (149.6); 456 (202.6); 531 (21.0); 574 (19.9); 644 (15.1); 700 (21.5); 795 (7.1). ^{1}H NMR (500 MHz, $CDCl_3$, 298 K): δ 9.11 (s, 1H); 8.81 (d, $^3J_{HH}$ = 5.0 Hz, 1H); 8.50 (d, $^3J_{HH}$ = 5.0 Hz, 1H); 8.40 (s, 2H); 8.27 (s, 1H); 8.24 (d, $^3J_{HH}$ = 5.0 Hz, 1H); 8.15 (d, $^3J_{HH}$ = 7.6 Hz, 2H); 8.09 (d, $^3J_{HH}$ = 5.0 Hz, 1H); 7.98 (d, $^3J_{HH}$ = 5.0 Hz, 1H); 7.89 (d, $^3J_{HH}$ = 7.6 Hz, 2H); 7.86 (d, $^3J_{HH}$ = 5.0 Hz, 1H); 7.85 (d, $^3J_{HH}$ = 5.0 Hz, 1H); 7.82 (d, $^3J_{HH}$ = 5.0 Hz, 1H); 7.80 (d, $^3J_{HH}$ = 7.0 Hz, 2H); 7.70 (d, $^3J_{HH}$ = 8.2 Hz, 2H); 7.68 (d, $^3J_{HH}$ = 8.2 Hz, 2H); 7.62 (d, $^3J_{HH}$ = 7.5 Hz, 2H); 7.60 (d, $^3J_{HH}$ = 5.0 Hz, 1H); 7.55 (d, $^3J_{HH}$ = 7.5 Hz, 2H); 7.48 (d, $^3J_{HH}$ = 6.9 Hz, 2H); 7.42 (d, $^3J_{HH}$ = 4.8 Hz, 1H); 7.37 (d, $^3J_{HH}$ = 7.5 Hz, 2H); 7.31 (d, $^3J_{HH}$ = 7.5 Hz, 2H); 7.07 (d, $^3J_{HH}$ = 7.3 Hz, 2H); 7.02 (b, 2H); 6.90 (d, $^3J_{HH}$ = 6.9 Hz, 2H); 6.7 (t, $^3J_{HH}$ = 7.6 Hz, 1H); 6.60 (t, $^3J_{HH}$ = 7.6 Hz, 1H); 6.38 (d, $^3J_{HH}$ = 7.6 Hz, 1H); 5.90 (d, $^3J_{HH}$ = 7.6 Hz, 1H); 5.27 (s, 2H); 4.68 (s, 2H); 2.70 (s, 3H); 2.67 (s, 3H); 2.62 (s, 6H); 2.56 (s, 3H); 2.52 (s, 3H); 2.09 (s, 3H); 2.07 (s, 3H). HRMS (ESI+): *m*/*z* 1603.478 (observed); 1603.475 (calculated for $[C_{104}H_{78}N_8AgNi]^+$).

Acknowledgment. Financial support from the Ministry of Science and Higher Education (Grant PBZ-KBN-118/T09/2004) is kindly acknowledged.

Supporting Information Available: Crystallographic data of **11** in CIF format, optical and CD spectra of bis(zinc) complex **7b** treated with aqueous potassium mandelate. This material is available free of charge via the Internet at http://pubs.acs.org.

IC800591N